Statistical analysis of storm electrical discharges reconstituted from a lightning mapping system, a lightning location system, and an acoustic array

Louis-Jonardan Gallin, Thomas Farges, Régis Marchiano, François Coulouvrat, Eric Defer, William Rison, Wolfgang Schulz, Mathieu Nuret

▶ **To cite this version:**

Louis-Jonardan Gallin, Thomas Farges, Régis Marchiano, François Coulouvrat, Eric Defer, et al.. Statistical analysis of storm electrical discharges reconstituted from a lightning mapping system, a lightning location system, and an acoustic array. Journal of Geophysical Research: Atmospheres, 2016, 121 (8), pp.3929-3953. 10.1002/2015JD023745 . hal-01316706

HAL Id: hal-01316706

https://hal.sorbonne-universite.fr/hal-01316706

Submitted on 17 May 2016

HAL is a multi-disciplinary open access archive for the deposit and dissemination of scientific research documents, whether they are published or not. The documents may come from teaching and research institutions in France or abroad, or from public or private research centers.

L'archive ouverte pluridisciplinaire **HAL**, est destinée au dépôt et à la diffusion de documents scientifiques de niveau recherche, publiés ou non, émanant des établissements d'enseignement et de recherche français ou étrangers, des laboratoires publics ou privés.

AGU PUBLICATIONS

JGR

Journal of Geophysical Research: Atmospheres

RESEARCH ARTICLE
10.1002/2015JD023745

Key Points:
- Natural lightning has successfully been reconstructed with a software used in infrasound research
- There is a good statistical fit between acoustic detections and VHF detections
- There is a good agreement between acoustic and VLF detections for lower sections of flashes

Supporting Information:
- Supporting Information S1

Correspondence to:
L.-J. Gallin,
gallin@dalembert.upmc.fr

Citation:
Gallin, L.-J., T. Farges, R. Marchiano, F. Coulouvrat, E. Defer, W. Rison, W. Schulz, and M. Nuret (2016), Statistical analysis of storm electrical discharges reconstituted from a lightning mapping system, a lightning location system, and an acoustic array, *J. Geophys. Res. Atmos.*, *121*, doi:10.1002/2015JD023745.

Received 2 JUN 2015
Accepted 14 MAR 2016
Accepted article online 21 MAR 2016

©2016. American Geophysical Union. All Rights Reserved.

Statistical analysis of storm electrical discharges reconstituted from a lightning mapping system, a lightning location system, and an acoustic array

Louis-Jonardan Gallin[1,2], Thomas Farges[1], Régis Marchiano[2], François Coulouvrat[2], Eric Defer[3], William Rison[4], Wolfgang Schulz[5], and Mathieu Nuret[6]

[1]CEA, DAM, DIF, Arpajon, France, [2]Sorbonne Universités, UPMC Univ Paris 06, CNRS, Institut Jean Le Rond d'Alembert UMR 7190, Paris, France, [3]LERMA, Observatoire de Paris, Paris, France, [4]New Mexico Institute of Mining and Technology, Socorro, New Mexico, USA, [5]OVE, Vienna, Austria, [6]Météo-France CNRM/GMME/MICADO, Toulouse, France

Abstract In the framework of the European Hydrological Cycle in the Mediterranean Experiment project, a field campaign devoted to the study of electrical activity during storms took place in the south of France in 2012. An acoustic station composed of four microphones and four microbarometers was deployed within the coverage of a Lightning Mapping Array network. On the 26 October 2012, a thunderstorm passed just over the acoustic station. Fifty-six natural thunder events, due to cloud-to-ground and intracloud flashes, were recorded. This paper studies the acoustic reconstruction, in the low frequency range from 1 to 40 Hz, of the recorded flashes and their comparison with detections from electromagnetic networks. Concurrent detections from the European Cooperation for Lightning Detection lightning location system were also used. Some case studies show clearly that acoustic signal from thunder comes from the return stroke but also from the horizontal discharges which occur inside the clouds. The huge amount of observation data leads to a statistical analysis of lightning discharges acoustically recorded. Especially, the distributions of altitudes of reconstructed acoustic detections are explored in detail. The impact of the distance to the source on these distributions is established. The capacity of the acoustic method to describe precisely the lower part of nearby cloud-to-ground discharges, where the Lightning Mapping Array network is not effective, is also highlighted.

1. Introduction

Most of studies about thunder were performed from 1960 to 1985. Thunder can be audible from lightning flashes at distances less than 25 km [*Fleagle*, 1949]. *Rakov and Uman* [2003] summarized the main characteristics of thunder. The induced pressure variations range from 0.1 to 10 Pa when observed several kilometers away from the lightning. The pressure wave is generally composed of several pulses, each lasting from 0.2 to 2 s, with a gap of duration 1 to 3 s between them. The overall duration of a single thunder event is several tens of seconds. The spectral content of thunder is between 10 Hz and 200 Hz [*Few*, 1969; *Holmes et al.*, 1971]. *Holmes et al.* [1971] showed that audible signal, with a frequency content from 50 Hz to 200 Hz, is first recorded and is then followed by pulses of frequencies below 20 Hz. Different physical processes have been proposed to explain thunder and its spectral content [e.g., *Few*, 1986]. There is still a debate on the mechanism explaining infrasound from thunder which is beyond the purpose of the present paper; *Pasko* [2009] reviewed of the published results on this subject. For the last 20 years, new studies about thunder have been published. They benefited from the development of lightning location systems based on electromagnetic measurements since the end of the 1980s. For instance, it was showed [*Assink et al.*, 2008; *Farges and Blanc*, 2010] that thunder can be detected at distances beyond 50 km using an infrasound array and that thunderstorm cells can be monitored in the vicinity of acoustic stations.

The first characterizations of the geometry of lightning channels were performed during the 1970s–1980s. They were based on the analysis of thunder records over acoustic arrays. Using a 30 m side network, along with a cross-correlation technique, *Few* [1968, 1970] succeeded in reconstructing the geometry of several flashes. These studies showed that a flash (being either a cloud-to-ground (CG) or an intracloud (IC)) presents an important horizontal extension (of several tens of kilometers) inside the thunderclouds. Results of acoustic reconstructions of lightning were compared to photographies of the corresponding events captured by a

Table 1. Previous Thunderstorm Studies

Authors	Acoustic Data
Teer and Few [1974]	17 CG and 20 IC [Arizona storm, also studied in *MacGorman et al.* 1981]
MacGorman et al. [1981]	statistics on three storms: Arizona (26 + 11 flashes), Colorado (35 flashes), and Florida (9 flashes)
Arechiga et al. [2011]	two triggered lightning flashes
Johnson et al. [2011]	at least 24 natural lightning flashes
Qiu et al. [2012]	two natural lightning flashes
Bodhika et al. [2013]	two natural lightning flashes, no comparison with LMA
Arechiga et al. [2014]	two intracloud natural lightning flashes
Anderson et al. [2014]	eight natural lightning flashes

camera [*Few and Teer*, 1974]. The authors found a good agreement between the acoustic reconstructions and the pictures when the discharge is visible, being outside the storm cloud. When CGs are considered, the visible vertical extension of the return strokes between the lower part of the thundercloud and the ground is only about 2 km to 3 km high. Acoustic reconstruction showed that the CG channel is still present inside the cloud but is invisible for optical devices. This limited the validation tests of any acoustic reconstruction method by cross comparison to optical observations. The same study [*Few and Teer*, 1974] evaluated the accuracy of their reconstruction method. They insisted on the importance of the knowledge of the local wind profile which is taken into account by a ray tracing propagation program to calculate the 3-D location of the acoustic source.

The significant horizontal extension of flashes was confirmed through statistical studies of reconstructed acoustic sources by *Teer and Few* [1974] and *MacGorman et al.* [1981]. This last work [*MacGorman et al.*, 1981] showed 3-D maps of acoustic sources from thunder and analyzed the statistical distribution of altitudes of the reconstructed sources inside thunderclouds. They found that acoustic sources were distributed in either one or two layers in the thunderstorms they analyzed. To explain this difference with the classical dipolar scheme inside the thundercloud, different points have to be taken into account as for instance the propagation of the acoustic wave, the acoustic radiation of the lightning channel, and its radiation pattern.

Presently, the acoustic reconstruction of lightning channels rekindled an interest. Acoustic method results can be compared to reconstructed geometries of discharges provided by high resolution electromagnetic detection networks such as a Lightning Mapping Array (LMA, see its description section 2.1). A great challenge here is to be able to compare the data coming from different technologies because an acoustic source cannot be necessarily directly associated to a VHF electromagnetic source.

Different authors [*Arechiga et al.*, 2011; *Johnson et al.*, 2011; *Qiu et al.*, 2012; *Bodhika et al.*, 2013] compared the results of acoustic reconstructions of lightning channels to electromagnetic ones. It is to be noted that all these papers focused on the comparison of reconstructions from acoustic records and VHF sources detected by a LMA. Table 1 lists previous published flash studies. Except in *Johnson et al.* [2011], reconstruction technique was adapted from the one developed by *MacGorman et al.* [1981]. Note that *Johnson et al.* [2011] described the positions of reconstructed thunder sources through continuous spatial distributions representing the coherency of the positions. These authors confirmed that the location of acoustic sources corresponded with the location of VHF sources.

The determination of uncertainties associated to acoustic reconstructions is an active research field: *Arechiga et al.* [2014] and *Anderson et al.* [2014] discussed the impact of meteorological profiles on localization.

The objective of this paper is to investigate acoustic reconstruction of a large number of *natural* thunder sources in the frequency range from 1 Hz to 40 Hz, covering both infrasound and low audible spectrum. Data are obtained from a 2 months observation period in southern France, with special emphasis here on a single day (26 October 2012). The storm lasted more than 4 h, with significant meteorological changes which made it impossible to obtain meteorology and especially wind profiles with sufficient precision over the observation period. Therefore, a very simple assumption of straight-line acoustic propagation is made.

The reconstructions present enough data to establish quantitative statistics of the spatial distribution of thunder sources, which are compared to those obtained by *MacGorman et al.* [1981].

The field campaign for the study of atmospheric electrical activity, during which natural thunder events were observed, is detailed along with the instrumentation in section 2. The method for acoustic reconstruction of natural lightning from thunder records is explained in section 3. Some examples of natural lightning (with both CGs and ICs), reconstructed by the acoustic method, are then presented in section 4. Since acoustic reconstruction is performed for more than 50 flashes, a statistical analysis of acoustic thunder sources localizations is carried out in section 5.

The large impact of propagation distances on the statistical distribution of altitudes of reconstructed acoustic sources is clearly demonstrated. Finally, the paper outlines the ability of the acoustic method to describe precisely the lower part of CGs when sufficiently close to the acoustic station. Since a lot of acronyms are used in the paper, a glossary lists them in Appendix A.

2. Description of the Measurement Campaign

The European HyMeX project [*Drobinski et al.*, 2014; *Ducrocq et al.*, 2014] aims at enhancing the understanding and the description of the water cycle and its changes in the Mediterranean region. From 2010 to 2020, it involves both field observation campaigns and numerical simulations from existing meteorological models. The observational data and the outputs corresponding to the numerical simulations are available online on the HyMeX database (http://mistrals.sedoo.fr/HyMeX/).

Correlations between lightning activity and precipitation rates during severe weather events being observed [e.g., *Pineda et al.*, 2007; *Dietrich et al.*, 2011], different research groups provide to the HyMeX community observations and outputs of numerical models for the electrical atmospheric activity during thunderstorms [*Defer et al.*, 2015]. Either existing operational instruments or specially deployed ones are used. The main goal is to characterize the electrical activity in the Mediterranean basin over several years.

A special observation campaign named SOP1 (Special Observation Period 1) took place within HyMeX in autumn 2012 (from 5 September 2012 to 6 November 2012) in the southeast of France (Figure 1a). The European Cooperation for Lightning Detection (EUCLID) operational lightning location network [*Schulz et al.*, 2014a, 2014b] provides detection data in the very low to low electromagnetic frequency range (VLF/LF) up to 350 kHz. A very high frequency (60 MHz–66 MHz) detection network, or Lightning Mapping Array (LMA), was installed for the first time in France, as described in section 2.1. It is here referred as "HyLMA." A microbarometer array (MBA) and a microphone array (MPA) were installed in order to record acoustic signatures associated to lightning flashes. They are described in section 2.2.1. *Defer et al.* [2015] detail more in depth the instrumentation deployed for the campaign and the operational status of the different sensors during the period. They summarize the first insights of the large amount of data recorded and identify the days where interesting atmospheric events were observed.

2.1. HyLMA Network

The HyMeX Lightning Mapping Array (HyLMA) is a network of 12 antennas designed to record very high frequency electromagnetic impulses (VHF, 60 MHz–66 MHz) generated by discharges inside a thundercloud [*Rison et al.*, 1999; *Krehbiel et al.*, 2000]. The usual diameter of a deployed array is 60 km. For the one deployed for the HyMeX-SOP1 campaign, the location of the antennas is given in Figure 1b inside a 100 km side square zone.

Such a network can map the geometry of lightning channels created by discharges with high spatial and temporal resolution. The antennas are equipped with GPS modules to guarantee the time reference. For each antenna, power is supplied by solar panels, which ensures the complete autonomy of each network point. "Time-of-arrival" technique is used to construct the geometry of the observed lightning discharges from the records at each antenna. *Koshak et al.* [2004] and *Thomas et al.* [2004] present in detail the postprocessing method used and the performances of the network. The authors show that the time error is about 50 ns. For sources within the network, the localization error on the altitude varies between 20 m and 30 m and between 6 m and 12 m for horizontal position.

2.2. Acoustic Records

2.2.1. Acoustic Station

An acoustic station was deployed for the SOP1 campaign from 27 August 2012 to 21 November 2012 near the airfield of Uzès (Gard, France, Figure 1a). It was located inside the HyLMA best resolution coverage zone (Figure 1b). It was composed of a microbarometer array (MBA) and a microphone array (MPA). The selected

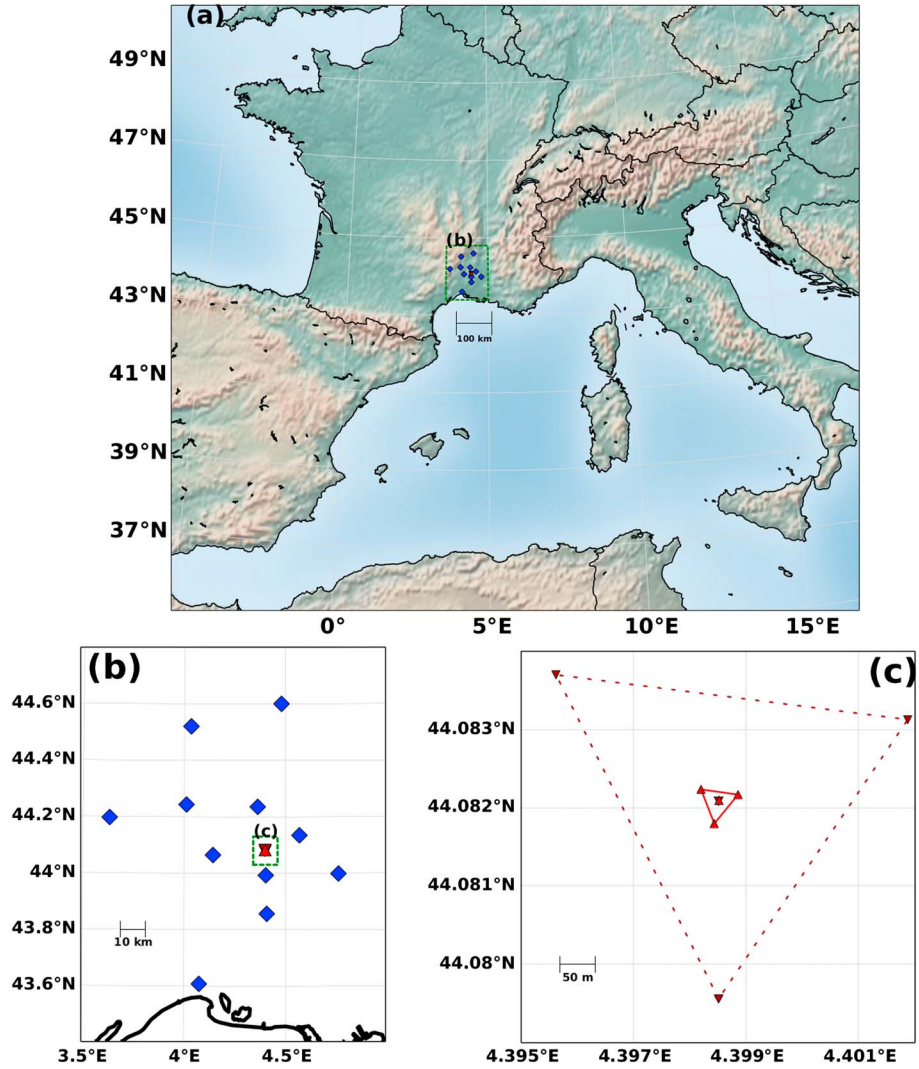

Figure 1. (a) Location of the HyLMA network and acoustic station in south of France (green rectangle, noted (b)). (b) Zoom around location of the 11 active HyLMA antennas (LMA antennas: blue diamonds and acoustic sensors: red triangles) (green rectangle, noted (c)). (c) Zoom on the Commissariat à l'Energie Atomique et aux Energies Alternatives (CEA) acoustic arrays, dashed lines: MBA, solid lines: MPA.

location corresponds to a flat terrain with a mean altitude of 260 m. Around the acoustic station, the vegetation efficiently filters the wind-induced noise. Noise due to human activity is limited in the neighboring area with low traffic from nearby roads and small villages.

The MPA was composed of four microphones, organized as a triangle of 50 m side. The MBA was composed four MB2005 microbarometers [*Ponceau and Bosca*, 2009], organized as a triangle of 500 m side centered around the first one (see Figure 1c). The central microbarometer (MB1) and the central microphone (MP1) were colocalized. GPS coordinates of each microbarometer and microphone are given in Table 2.

In this paper, only the records from the MPA are considered. Indeed, the MPA dimensions correspond to wavelengths ranging from infrasounds to low audible contents (see Table 3), it is well adapted to cover the selected 1 Hz–40 Hz frequency band. The MBA dimensions turn out to be too large to correctly detect coherent wavefronts of the considered frequency contents. This statement is in agreement with the results established by *Farges and Blanc* [2010]. Thus, thunder signatures recorded with the MBA are not explored in this paper.

The microphones used are the MCB2006. A simplified "rosette pipe filter" [*Hedlin et al.*, 2003; *Alcoverro and Le Pichon*, 2005; *Walker and Hedlin*, 2009] was used to reduce local noise over a microphone. The accessible

Table 2. GPS Coordinates of the MBA Sensors and the MPA Sensors

Point	Longitude	Latitude
MB1	4° 23′ 54.6″E	44° 4′ 55.5″N
MB2	4° 23′ 44.2″E	44° 5′ 01.3″N
MB3	4° 24′ 06.7″E	44° 4′ 59.3″N
MB4	4° 23′ 54.6″E	44° 4′ 46.4″N
MP1	4° 23′ 54.7″E	44° 4′ 55.6″N
MP2	4° 23′ 53.5″E	44° 4′ 56.0″N
MP3	4° 23′ 55.9″E	44° 4′ 55.8″N
MP4	4° 23′ 54.4″E	44° 4′ 54.5″N

frequency range of the microphone is from 10^{-1} Hz to 10^4 Hz in laboratory measurements. During the SOP1, the sampling frequency was 500 Hz. Each measurement point was independent and was equipped with a GPS module to insure absolute dating. The digitizing and the storage of the data were done locally. Each measurement point of the array was powered from seven batteries.

Figure 2 shows the power spectral density of background noise for the four MPA measurement points. It clearly shows microphones resonance between 20 and 150 Hz. In the field, a protection against humidity led to the appearance of a broadband resonance from 80 Hz to 120 Hz with a maximum around 100 Hz. There also exist very narrow peaks at 25, 40, 50, and 70 Hz. We thus choose here to work on a limited frequency band from 1 Hz to 40 Hz. This choice enables the study of both near infrasounds and low audible frequencies. The lower limit of 1 Hz filters out the effect of the swell from the Atlantic, and the upper limit avoids most of the resonances from the measurement system.

2.2.2. Data Processing

The acoustic records are processed by the automatic progressive multichannel cross-correlation (PMCC) algorithm [*Cansi*, 1995; *Brachet et al.*, 2009]. It was initially developed to automatically detect seismic events. *Cansi and Le Pichon* [2009] recall that when the wavelengths of the signals recorded by each point of an acoustic array are approximately equal to the size of the array, the latter is referred as being a miniarray. In this case, waveforms are expected to remain highly coherent while traveling across the array. Advantage can then be taken from this to compute differences between times of arrival over pairs of sensors with signal processing techniques based on the maximum of cross correlation. An overview of the postprocessing method can be found in supporting information and the detailed algorithm is described by *Caljé* [2005]. In practice the computation is done on small sliding time windows and by frequency bands. This defines an ensemble of time frequency two-dimensional boxes. The duration of time windows is adapted to the corresponding frequency band. For the present study, the chosen settings are presented in Table 4. The overlapping of the sliding time windows was chosen equal to 50% for all frequency bands. Coherent transient signals over the array are

Table 3. Top: Infrasonic Frequencies Associated to Characteristics Lengths (Side Length and Center-Apex Distance) of the MPA and the MBA[a]

	MPA	MBA
Side	50 m	500 m
Characteristic frequency	6.8 Hz	0.68 Hz
Center to apex distance	28 m	288 m
Characteristic frequency	12 Hz	1.2 Hz
Wind reducing pipe filter associated to each sensor		
Shape	four straight pipes	four Y-shaped pipes
Length of pipes	40 cm	1 m each branch
Induced resonance frequency	200 Hz	30 Hz
Resonance amplitude	+35 dB	+14.5 dB

[a]For a given length, the frequency is established by dividing the ground sound speed $\overline{c}_0$ by this length. Bottom: wind pipe filters characteristics.

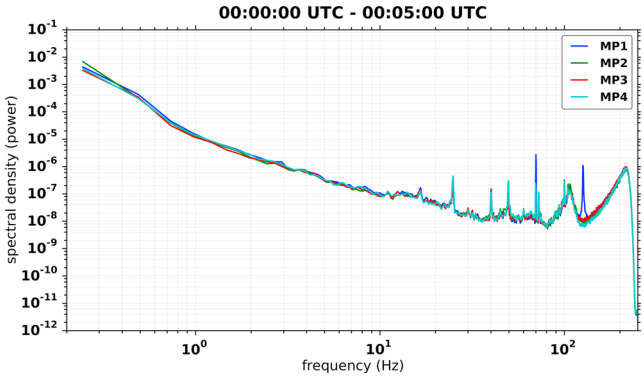

Figure 2. Power spectral density of the background noise recorded during the night on the 26 October 2012 by the four microphones of the MPA. The time duration is of 300 s (5 min).

searched in each of these two-dimensional boxes. When a box contains a coherent detection, the algorithm outputs its time and frequency limits [*Le Pichon et al.*, 2010], the azimuth and horizontal trace velocity of the signal, the root-mean-square amplitude of the detection, its consistency and at last its correlation.

2.3. Comparison of HyLMA and Acoustic Detections

During the 2 months observation period, systematic exploration of EUCLID observations showed that several thunderstorms passed just over the station. The selected thunderstorms have to be close enough to the MPA to optimize the observation conditions. *Farges and Blanc* [2010] showed that for acoustic sources farther than 50 km, the acoustic detectability turns out to be very weak. Furthermore, stormy days which were not too active have to be selected. Indeed, a flash with a horizontal extension of 20 km would correspond to an acoustic time delay at the receiving array of about 58 s (assuming $\bar{c}_0 = 340$ m/s). This means that successive flashes from which thunder signatures are recorded at the station must be separated from one another by at least 1 min, so that different acoustic signatures do not overlap.

Figure 3 presents EUCLID observations up to 100 km around the acoustic station for 3 days during SOP1. On 24 September 2012, a very active storm moving from northwest to southeast, occurred from 0 UTC to 10 UTC (13070 EUCLID observations). It moved toward the acoustic station from 0 UTC to 2 UTC. From 2 UTC to 6 UTC, the storm was less than 20 km away from MPA. From 6 UTC to 10 UTC, the storm moved away eastward. This day was studied by *Defer et al.* [2015] and some acoustic data were briefly analyzed. Electrical activity from a weaker daily lightning rate on 25 September 2012 (790 EUCLID observations, from 9 UTC to 17 UTC) is presented in Figure 3b. This event could have been selected for a detailed study, but it encompasses a narrow range of azimuths (from southwest to northeast, Figure 3b). This case would prevent investigating acoustic signals coming from a wide set of azimuths. The 26 October 2012 case was selected for thorough study in this

Table 4. PMCC Settings, Lengths of the Time Windows, and Boundaries of the Frequency Bands

Time Windows, Length (s)	Frequency Bands (Hz)
5.0	1–4.9
4.5556	4.9–8.8
4.1111	8.8–12.7
3.6667	12.7–16.6
3.2222	16.6–20.5
2.7778	20.5–24.4
2.3333	24.4–28.3
1.8889	28.3–32.2
1.4444	32.2–36.1
1.0	36.1–40

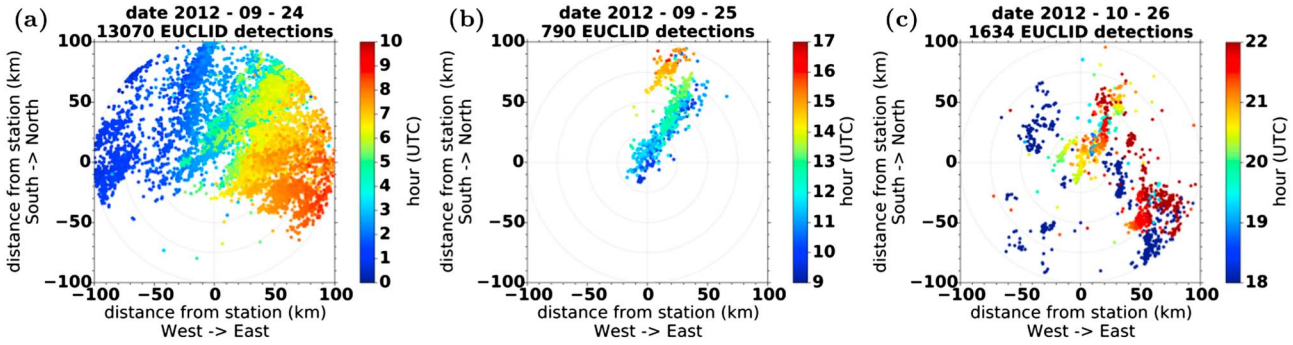

Figure 3. Location of the EUCLID observations around the acoustic station. The colorbar represents the hour of the day (UTC) in a time window framing the storm. (a) 24 September 2012, (b) 25 September 2012, and (c) 26 October 2012.

paper because this thunderstorm was close to the acoustic station (less than 20 km, Figure 3c) from 18 UTC to 22 UTC. It was moderately active (1634 observations from EUCLID) and covered all the azimuths relative to the MPA during this time period.

Along with the constructed set of acoustic detections from thunder waveforms, the electromagnetic detections of discharges are available both from the HyLMA and EUCLID networks. The assumption is made that the detected lightning flashes represent possible acoustic sources. A simple hypothesis of homogeneous propagation directly from these potential sources toward the MPA is then introduced. The homogeneous speed of sound is considered to be the ground effective sound speed $\bar{c}_0 = 340$ m/s at the station (see section B). This value is deduced from the analysis of temperature profiles around the acoustic station given by the reanalysis of weather simulations computed by the AROME-WMED software (AROME West-MEDiterranean region) [*Fourrié et al.*, 2015]. It is a version of the operational weather forecast model AROME from Météo-France [*Seity et al.*, 2011], specifically adapted for HyMeX. *Farges and Blanc* [2010] showed that a

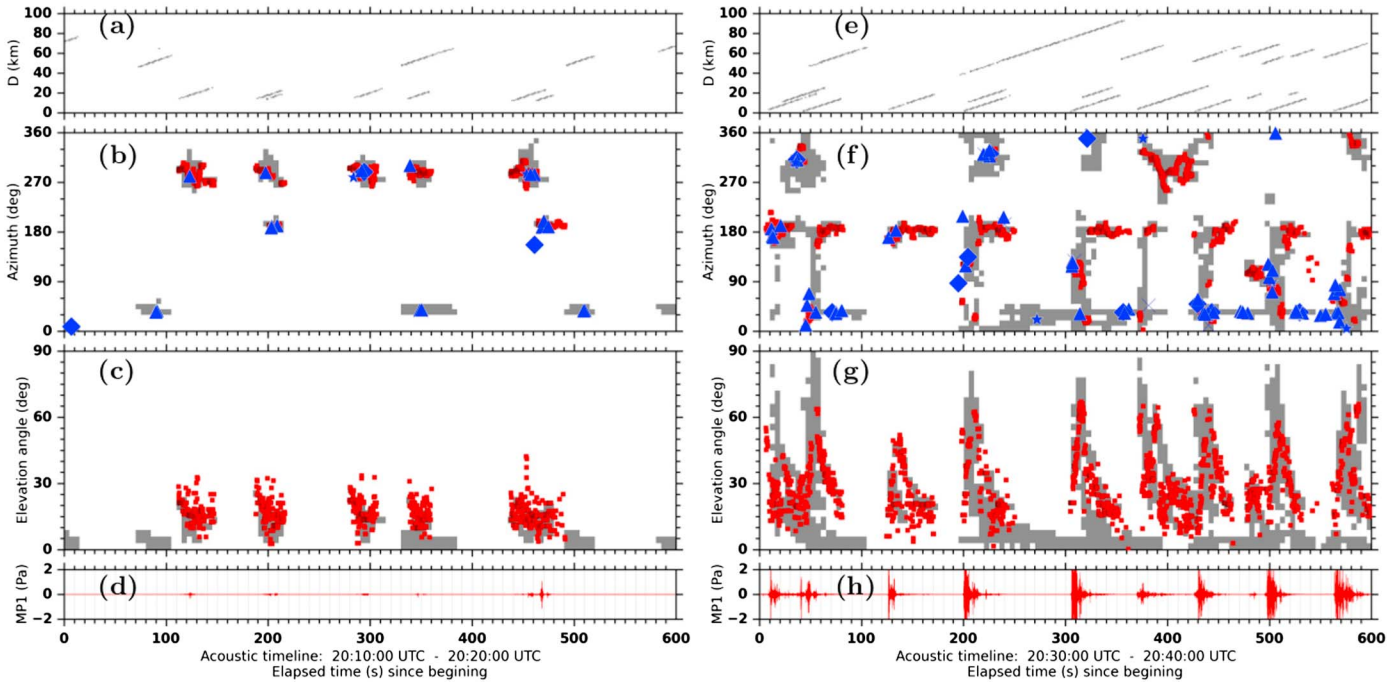

Figure 4. Exploratory views (left) from 20:10 UTC to 20:20 UTC and (right) from 20:30 UTC to 20:40 UTC. In red, acoustic (e.g., PMCC) detections. In gray, HyLMA detections integrated in intervals of 5 s, 10° in azimuth, and 3° in elevation angle. Blue symbols: EUCLID observations (triangle symbol: negative CG, cross: positive CG, diamond: negative IC, and star: positive IC). (a, e) Straight distance *D* between HyLMA detections and the MPA center. Each segment is the extension (in distance from the MPA) of a discharge, the most remote parts of the discharge arriving the last at the station. (b, f) Azimuths of the HyLMA, the acoustic, and the EUCLID observations. (c, g) Elevation angles of the HyLMA and the acoustic detections. (d, h) Acoustic signal recorded at the central microphone (MP1).

wind at ground level which is too strong affects the acoustic detectability (see Figure 13 of their paper). As it will be shown, comparisons with flashes mapped by the HyLMA showed our acoustic reconstructions were reasonably consistent with them, but we hope later to explore the effects of the wind around the station more thoroughly. Following this, the spatial coordinates of electromagnetic detections are expressed in Cartesian coordinates relative to the center of the acoustic station. Their azimuths are then computed. Since EUCLID observations do not have any notion of altitude, elevation angles of the sources at the acoustic station are computed for the HyLMA records only. Considering that electromagnetic detections are potential acoustical sources, presumed time of arrival at the center of the acoustic station are established using the times of the electromagnetic detections, the straight distances from the sources to the MPA and the sound speed value at ground level $\overline{c}_0$.

Using the time at the acoustic station as a common reference axis, HyLMA, EUCLID, and acoustic detections are plotted. Figure 4 shows an example of a such comparison for 26 October 2012 around 20 UTC. From 20:10 UTC to 20:20 UTC, Figure 4b shows two flashes were produced south of the MPA and five flashes northwest of the MPA. The electromagnetic sources of these seven flashes are less than 40 km away from the MPA (Figure 4a). It is noted that for these events, the agreement between the azimuths of the electromagnetic detections and the ones from MPA is excellent, similar to the agreement obtained in *Farges and Blanc* [2010]. Each gray region corresponds to one or more EUCLID observations. Four other flashes were in the northeast azimuth, and one was in the north azimuth. They are more distant (more than 40 km) and PMCC is not able to detect any acoustic signal from these flashes (Figure 4a).

The elevation angles at the acoustic station of the HyLMA detections and the acoustic ones are plotted in Figure 4c. The agreement on the elevation angles is good between HyLMA and PMCC detections. Since the five HyLMA flashes at the northwest of the MPA and the two HyLMA flashes at the south of the MPA are about 20 km in distance, the elevation angles are small (between 5° and 30°). In this plot, the two flashes arriving at the acoustic station between the times 200 s and 240 s (Figure 4c) are not differentiable from one another since they correspond to the same acoustic times. For the five most remote flashes, the elevation angles of the corresponding HyLMA detections are close to the horizon (between 0° and 10°) and the acoustic signal is very weak (Figure 4d).

From 20:30 UTC to 20:40 UTC, the storm is just over the acoustic station (Figure 4e). A group of 14 flashes is produced at less than 30 km away from the MPA. They are in the south azimuth and extend to the north passing through the east (Figure 4f). The HyLMA sources which are above the MPA present elevation angles varying up to 90°. Elevation angles for acoustic detections cover a smaller range (from 5° to 70°). PMCC detects few sources on the horizon and none at the vertical of the MPA. For elevation angles between 10° and 70°, the agreement between the HyLMA detections and the acoustic ones is excellent (Figure 4g). Finally, the acoustic signal shows nine distinct impulsive signals (Figure 4h). This is less than the 14 flashes detected by the HyLMA because acoustic signals emitted by these flashes can arrive at the same times on the acoustic station and thus can superimpose. Among the signals from different superposing sources, PMCC constructs detections only for the strongest and most coherent ones. This explains and justifies why we choose moderately active thunderstorm to validate our method, so that there is reduced masking effect of one lightning flash by another.

From this study, it is demonstrated and validated (against comparison to HyLMA detections) that the MPA along with PMCC used as postprocessing can follow wide variations of elevation angles, up to about 70°, although there is no acoustic detection below 5°.

Using these systematic exploration graphics such as Figure 4, plotted for the whole thunderstorm duration from 18:00 UTC to 22:00 UTC, a set of 56 flashes detected by all three instruments (HyLMA, EUCLID, and MPA) was selected during 26 October 2012. For these 56 events the correlation between the HyLMA and acoustic detections is visually excellent in azimuth and time (in the MPA reference). Misfits for the elevation angles of the acoustic detections can be present. The determination of elevation angles is more sensitive to errors as the angle becomes small. Propagation effects, especially those due to wind shear, can be also large at small elevation angles.

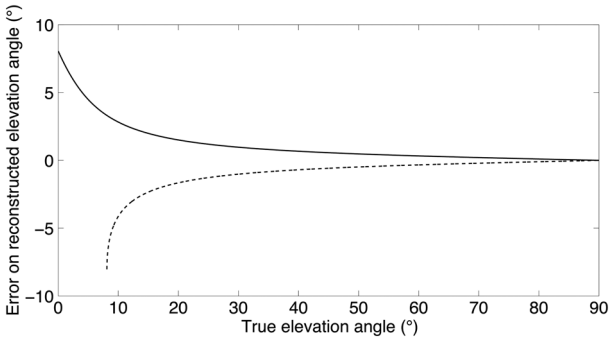

Figure 5. Absolute error (in degrees) between reconstructed and true elevation angles, versus true angle (in degrees), for a horizontal trace velocity overestimated (solid line) or underestimated (dashed line) by 1%. Overestimating (resp. underestimating) horizontal trace velocity is equivalent to underestimate (resp. overestimate) local sound speed.

3. Acoustic Reconstruction of Lightning Flashes

The flashes detected by the HyLMA network can be considered to be produced instantaneously compared to the characteristic acoustic propagation times. For one flash, characteristic durations of thunder records are typically about 1 min long (see Figures 4d and 4h). These long duration signals recorded at the MPA are due to the important spatial extension of the flashes (approximately 20 km horizontally and about 5 km to 8 km vertically), with the farthest sources contributing to the tail of the acoustic signal. The electromagnetic detection of the flash is chosen as the time of the event. More precisely, we chose here as time origin the time (noted t_{LMA_0}) of the first electromagnetic detection for a given flash. As the lightning rate is relatively low for the selected thunderstorm, there is no ambiguity in identifying all HyLMA sources that belong to a given flash. The elapsed time from the HyLMA detection to the time the corresponding acoustic detection was found by PMCC (denoted t_{PMCC}) determines both the propagation time Δt and the straight-line distance $D_{\mathbf{S}}$ from the source **S** of the acoustic signal to the station.

$$\begin{aligned} \Delta t &= t_{\mathrm{PMCC}} - t_{\mathrm{LMA}_0} \\ D_{\mathbf{S}} &= \bar{c}_0\, \Delta t. \end{aligned} \tag{1}$$

If a direct propagation is assumed, the azimuth θ of the PMCC detection (see equation (8) in the supporting information) is the azimuth $\theta_{\mathbf{S}}$ of the source **S**. The elevation angle $\phi_{\mathbf{S}}$ of the source is calculated using the following equation:

$$\cos\phi_{\mathbf{S}} = \frac{\bar{c}_0}{V_h}, \tag{2}$$

where V_h is referred as being the apparent horizontal velocity or horizontal trace velocity.

Having obtained the value $D_{\mathbf{S}}$ and knowing $\theta_{\mathbf{S}}$ and $\phi_{\mathbf{S}}$, one can construct the Cartesian coordinates $X_{\mathbf{S}}, Y_{\mathbf{S}}, Z_{\mathbf{S}}$ of the acoustic source **S** relatively to the acoustic station:

$$\begin{cases} X_{\mathbf{S}} = \bar{c}_0\, \Delta t\, \cos\phi_{\mathbf{S}}\, \sin\theta_{\mathbf{S}} \\ Y_{\mathbf{S}} = \bar{c}_0\, \Delta t\, \cos\phi_{\mathbf{S}}\, \cos\theta_{\mathbf{S}} \\ Z_{\mathbf{S}} = \bar{c}_0\, \Delta t\, \sin\phi_{\mathbf{S}}. \end{cases} \tag{3}$$

The elevation angle $\phi_{\mathbf{S}}$ is very sensitive to errors or uncertainties for low-elevation angles as the horizontal trace velocity gets close to sound speed. This is illustrated by Figure 5 showing the absolute error between the reconstructed and the true elevation angle. For establishing the plot, a $\pm 1\%$ error is assumed in equation (2), either for the measured horizontal trace velocity V_h or for the measured sound speed $\bar{c}_0$, relative to true values. For true elevation angles above 20°, the error remains small, less than 2°. However, for smaller angles, this error sharply increases up to several degrees. In case of underestimated horizontal trace velocity or overestimated sound speed, the reconstruction process breaks down for true angles below approximately 8°, as the erroneous ratio $\bar{c}_0/V_h$ then gets larger than one. In case of overestimated horizontal trace velocity or underestimated sound speed, the reconstruction process cannot predict angles below approximately 8°. This value

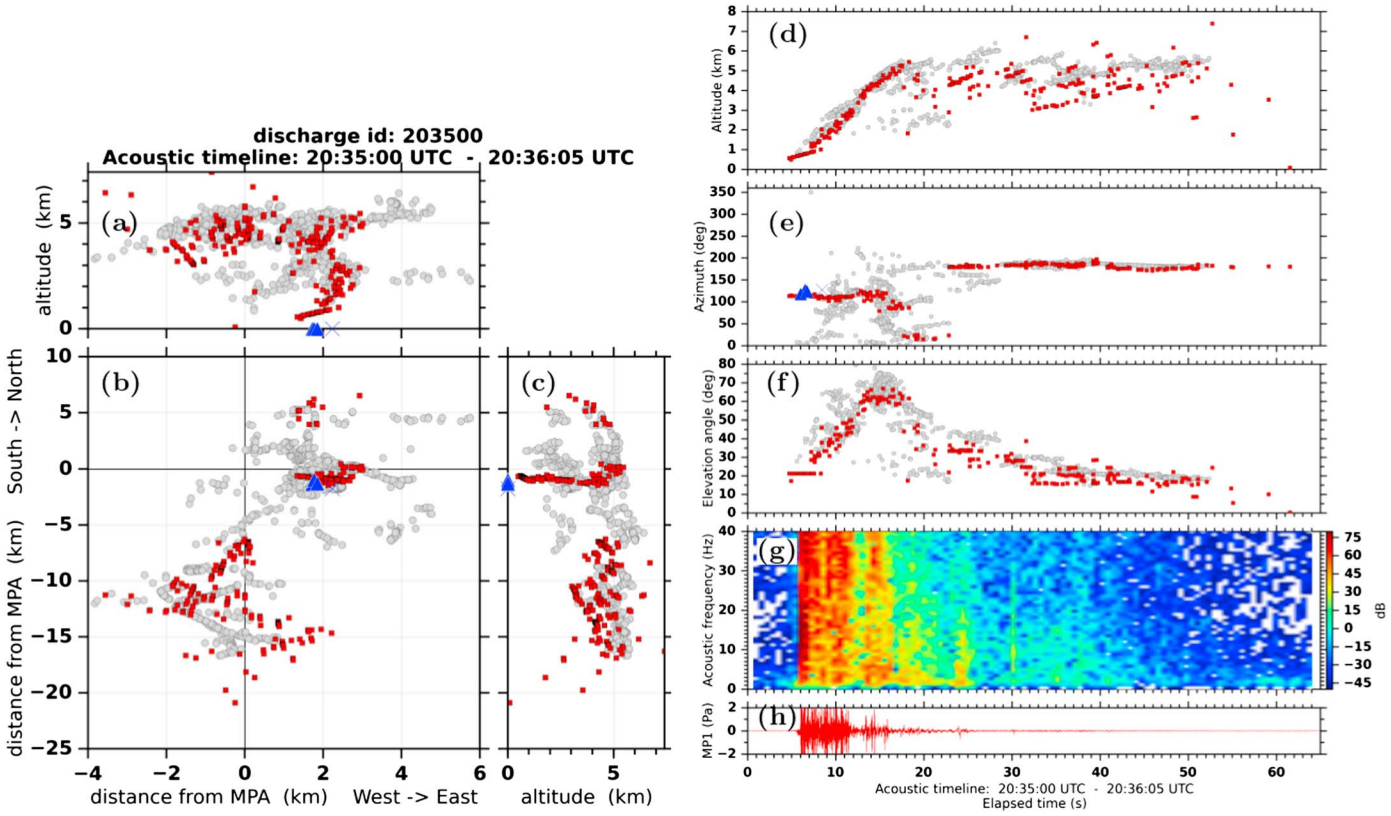

Figure 6. Acoustic reconstruction of the flash occurred on 26 October 2012 at 20:35:00 UTC. Grey dots: HyLMA detections, red squares: reconstructed acoustic detections, and blue symbols: EUCLID strokes from raw detections (with same symbols as in Figure 4). (a) Locations of HyLMA detections, EUCLID observations, and reconstructed MPA detections in longitude-altitude plane. (b) In longitude-latitude plane (MPA is at the origin). (c) In altitude-latitude plane. (d) Altitude of HyLMA and MPA detections versus time. (e) Azimuth of HyLMA, EUCLID, and MPA detections versus time. (f) Elevation angles of the HyLMA and MPA detections versus time. (g) Spectrogram of thunder signature at MP1. (h) Corresponding thunder signature at MP1 versus time.

of 8° is of course increasing with error made on measuring $\bar{c}_0$ or V_h. This may explain, why, as noticed before when examining (Figure 4g), very few acoustic signals gave elevation angles lower than 10°, while many more HyLMA detections were found with those elevation angles.

The direct propagation model neglects the variations of the effective speed of the sound (the combination of the sound speed and the wind velocity) with the altitude. On the contrary, a ray tracing approach takes into account simultaneously the variations of sound speed and of wind velocity with altitude. The trajectories of the retropropagated acoustic rays would then expected to be more precise than those calculated with a direct reconstruction. Note however that ray theory is a high-frequency approximation whose application at low frequencies is questionable. For the frequency bandwidth (1–100 Hz) and the propagation range (a few kilometers) over the ground here considered for thunder, numerical comparison between ray theory and simulations of nonlinear wave theory [*Gallin et al.*, 2014, see their Figure 12] showed a good agreement for highest frequencies (50 or 100 Hz), while the typical features of ray theory such as formation of shadow zones or waveguides get largely blurred at lower frequencies (10 Hz). Moreover, ray tracing requires an accurate description of the meteorological profiles at the time when thunder is recorded by MPA. For this campaign, we benefited from meteorological profiles provided by the AROME-WMED software (sound speed and wind over and around the MPA) with a spatial resolution of 2.5km × 2.5km horizontally and from ground level to 16 km in altitude using isobaric pressure levels (resolution of 50 hPa near the ground) and a temporal resolution of 1 h. As shown in the Appendix B, acoustic reconstruction has also been carried out using the ray tracing method. Results show that for sources nearby the MPA (distant from less than 10 km), the ray tracing approach does not provide any significant enhancement in terms of source localization compared to direct propagation assumption. For more distant sources (from 10 km to 30 km), a significant number of rays turn out to be strongly deviated upward. Also numerous sources are localized by ray tracing erroneously at ground level because of waveguide formation, while they would be expected within the thundercloud. This inadequacy

of ray theory in the present thunder study is likely due to two possible reasons: (1) errors in the temperature and wind along the ray path and (2) the acoustic frequency being too low to be treated well by ray tracing. Especially, the temporal variations of the meteorological profiles are likely to be locally significant over times scales much shorter than 1 h in case of stormy weather. Consequently, we decided to rely the present study on the direct reconstruction method, which turns out here more robust than the ray tracing one. The need for robustness is crucial in the frame of this paper because our main purpose is to establish statistics on acoustic reconstruction of lightning flashes compared to HyLMA reconstruction.

4. Observations and Case Study Analysis

4.1. Lightning Flashes Close to the Acoustic Station

To illustrate and validate the reconstruction method of natural lightning flashes, several case studies are presented. In Figure 6, a CG flash with one positive ground stroke and three negative ground strokes was recorded at 20:35:00 UTC near the MPA (see Table 5). According to HyLMA records, the flash lasted for 500 ms and the ground strokes occurred during the first 50 ms of the flash. Altitude of the VHF HyLMA sources did not exceed 6 km. The flash was distributed along the north-south direction. The connections to the ground are only 2 km away from the station.

The 3-D positions of the reconstructed acoustic points show that PMCC correctly detected the upper positive channels of the flash that were recorded during the second part of the flash life. It appears (Figures 6a and 6b) that the acoustic method followed very precisely the tilted path of the return strokes from a low altitude of 500 m up to 5 km into the cloud. Note that this is not the case for the HyLMA below 2 km altitude, for which very few detections are reconstructed. This point will be discussed further in section 5.2. There is an excellent agreement between the position of the return stroke located by the acoustic method and the localizations of EUCLID observations.

The MPA was not able to detect the horizontal layer at an altitude about 2 km: it has been masked by the detection of the more intense acoustic signal from the return stroke itself which arrives at the same acoustic times. In contrast the acoustic method has correctly detected the horizontal part of the flash which extends toward the south direction over a distance of 20 km, at an altitude of about 5 km (Figure 6b). Using the acoustic time as *x* axis, the stacked plots in Figures 6d–6f show the altitude of the HyLMA detections and the reconstructed acoustic detections. The flash occurred at 20:35:00 UTC and lasted less than 1 s, but the corresponding acoustic signal is much longer with a duration of about 1 min.

In Figures 6d and 6f, it is clearly shown that the acoustic signal from 5 s to 15 s is associated with the vertical part of the flash (assumed to be due to different return strokes). This corresponds to the burst in the thunder waveform in Figure 6h. The starting of this burst (at time 5 s) corresponds to the time of arrival of an acoustic content which is likely to have been emitted by the strokes detected by EUCLID (Figure 6e). During the time interval 5 s to 15 s, the acoustic method clearly followed the corresponding rapid increase of the elevation angles from about 15° up to 70°. Then, from 15 s to the end of the acoustic signal, the elevation angle decreases slowly as the flash extends horizontally from the acoustic station, in the south azimuth (Figure 6e). The acoustic waveform associated to the return strokes contains consecutive broadband acoustic pulses that cover the whole frequency band from infrasounds to audible frequencies with uniform energy (Figure 6g).

The return strokes being close to the MPA, propagation effects are negligible (this argument is illustrated by Figure B2 of Appendix B). It is thus concluded that the return strokes emit an important infrasonic contents below 20 Hz which has been recorded at the station. The spectrogram also shows that the return stroke is associated to the most intense part of the measured acoustical signal. From 15 s to 25 s, the spectral content is still broadband but with a smaller energy (about 60 dB less). Then from 25 s, the frequencies are driven toward infrasonic content below 20 Hz with a decreasing energy as the flash goes away from the MPA.

A second flash occurred at 20:35:58 UTC. It is a bilevel intracloud flash (see Table 5). Since it occurred less than 1 min after the flash described previously, the meteorological conditions remained the same. Figure 7 shows that the flash is organized in two horizontal layers (around altitudes 3 km and 8 km), linked by two vertical channels (visible in Figure 7a).

Analysis of the HyLMA records suggests that the studied flash looked like a regular bilevel normal polarity IC flash until the low-level positive reached the area of the second vertical channel where a new bilevel normal polarity IC flash was initiated and propagated at both levels with horizontal extensions up to 20 km.

Table 5. First Six Columns: Data From Raw EUCLID Detections for the Presented Flashes (26 October 2012)[a]

Time (UTC)	Lat (deg)	Lon (deg)	C (kA)	Type	E (km)	X (km)	Y (km)	θ (deg)	D_h (km)
20:35:00.07	44.066	4.426	18.5	CG	0.3	2.237	−1.742	127.9	2.836
20:35:00.07	44.070	4.420	−127.6	CG	0.2	1.725	−1.342	127.9	2.186
20:35:00.10	44.073	4.420	−29.5	CG	0.2	1.765	−0.953	118.4	2.006
20:35:00.13	44.070	4.421	−13.2	CG	0.2	1.845	−1.264	124.4	2.237
20:35:58.85	44.132	4.385	9.9	IC	0.89	−1.037	5.640	349.5	5.732
20:42:45.56	44.072	4.438	−12.9	IC	2.09	3.203	−1.041	108.0	3.368
20:42:45.57	44.068	4.441	−67.4	CG	0.2	3.467	−1.553	114.1	3.799
20:42:45.59	44.082	4.418	−13.5	CG	0.2	1.589	0.025	89.1	1.588
20:42:45.66	44.052	4.427	−11.1	CG	0.2	2.317	−3.288	144.8	4.024
20:42:45.73	44.088	4.412	−14.5	CG	0.2	1.086	0.670	58.3	1.273
20:49:03.34	44.163	4.409	−44.3	CG	0.2	0.845	9.020	5.3	9.057
20:49:03.53	44.065	4.368	−15.2	CG	0.3	−2.388	−1.887	231.6	3.046
21:16:54.17	44.238	4.644	−32.2	CG	0.4	19.573	17.367	48.4	26.165
21:16:54.17	44.231	4.657	−161.1	CG	0.2	20.659	16.614	51.1	26.508
21:16:54.21	44.250	4.631	−13.0	CG	0.2	18.566	18.698	44.7	26.347
21:16:54.62	44.254	4.579	−17.4	CG	0.2	14.415	19.233	36.8	24.032
21:16:54.72	44.175	4.372	10.7	IC	3.20	−2.073	10.366	348.6	10.569
21:24:01.93	43.596	4.968	−11.4	IC	1.1	45.885	−53.790	139.5	70.703
21:24:01.93	43.599	4.972	−131.6	CG	0.2	46.189	−53.510	139.2	70.689
21:24:01.97	43.625	4.981	−17.4	CG	0.2	46.941	−50.613	137.1	69.032

[a]The abbreviations "lat" and "lon" stand for "latitude" and "longitude," respectively. Variable C designates the peak current. The column named "type" differentiates cloud-to-ground strokes (letters "CG") from intracloud ones (letters "IC"). The variable "E" is the error associated to the detection. Last four columns: locations of EUCLID detections relatively to the MPA center. Column labeled X: Cartesian coordinates of the detection relatively to the MPA, in the west to east direction. Column Y: Cartesian coordinates of the detection relatively to the MPA, in the south to north direction. Column θ: azimuth of the detection. Column D_h: distance of the detection to the MPA center.

The acoustic method correctly detected the channels inside the cloud. In particular numerous acoustic detections are associated to the vertical elements of the flash. The two horizontal layers have also been detected acoustically but with less detections. The flash covered all the region above the acoustic station: all the azimuths were swept. The two horizontal layers of the flash are shown in Figures 7d and 7f. The HyLMA points are organized in the acoustic time as two layers. It is noted that the MPA cannot detect acoustic sources in both levels at the same time. Acoustic detections alternate between the upper or the lower layer of the flash. Since the acoustic sources associated to each of the two layers of discharges arrive at the same times on the acoustic network, they superpose in the recorded signal, but one dominates the MPA analysis. The end of the burst is of extremely low amplitude. Nonetheless, PMCC is able to extract coherent acoustic detections from the background noise. The availability of the HyLMA points clearly validates acoustic detections as being associated to the part of the flash which is the most distant relative to the MPA. The burst in the thunder signal from 10 s to 12 s (Figure 7h), corresponds to the observation by EUCLID of a positive IC (Figure 7e) in azimuth 350° at 11 s. The spectrogram (Figure 7g) is of much lower amplitude than in the previous case (30 dB less), but the signal still appears to be broadband, especially between the times 5 s to 20 s. The most energetic spectral peak is located in the infrasounds (below 10 Hz) at times between 8 s and 12 s. It corresponds to the time of the EUCLID intracloud flash detection (see the abscissa of the star symbol in Figure 7e).

Figure 8 is a synthetic view of the two presented flashes, where each reconstructed acoustic detection is colored by its acoustic amplitude and its time which are PMCC results. It is clear that the multiple acoustic detections, which are of large amplitude up to few tenths of Pascals (Figure 8a), correspond to vertically oriented discharges, probably due to return strokes. The acoustic signal emitted by most distant parts of the flash arrives at the end of the burst (Figure 8b). Its amplitude is very weak (few hundredths of Pascals, Figure 8a). For the case of the IC, the acoustic detection is of weaker amplitude (Figure 8c).

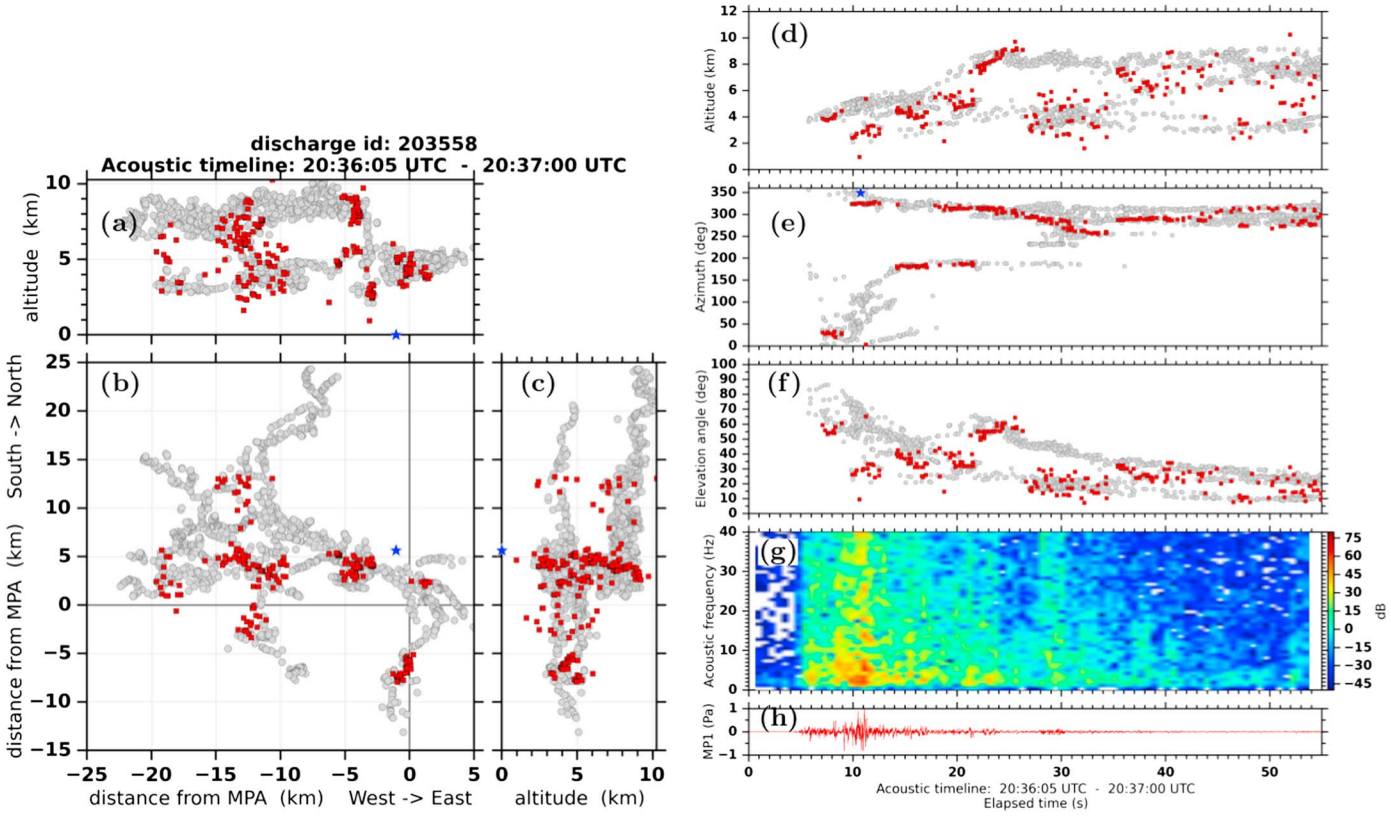

Figure 7. Acoustic reconstruction of the flash occurred on 26 October 2012 at 20:35:58 UTC. Same legend as in Figure 6.

4.2. Tracking Storm Cells

Figure 9 shows several synthetic views of the HyLMA, the EUCLID, and the MPA detections for different time windows of 10 min duration during the storm. The active cells were passing above the station, moving from southwest toward northeast. A cell was present in the northeast azimuth from the MPA, at about 25 km in horizontal distance (Figure 9a), and acoustic detections are correctly associated to it. Then this cell moved away in the same direction (Figures 9b–9d) but it was not detected acoustically anymore. In Figure 9d, again the effect of masking by acoustic sources very close from the MPA explains this fact. But this interpretation does not hold for the case presented in Figure 9b. On the contrary, a distant cell (between 50 km and 75 km

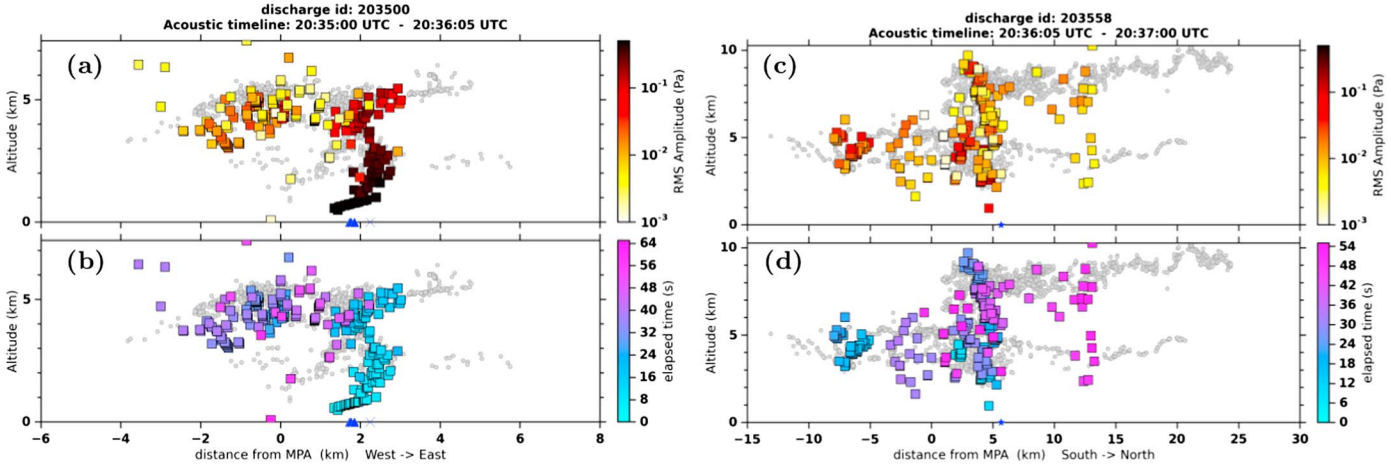

Figure 8. (a, b) Flash occurred on 26 October 2012 at 20:35:00 UTC in projection in the longitude-altitude plane. (b, d) flash occurred on 26 October 2012 at 20:35:58 UTC in projection in the latitude-altitude plane. Each reconstructed acoustic detection is colored with: amplitude (a, c) and elapsed time (b, d) of the detection.

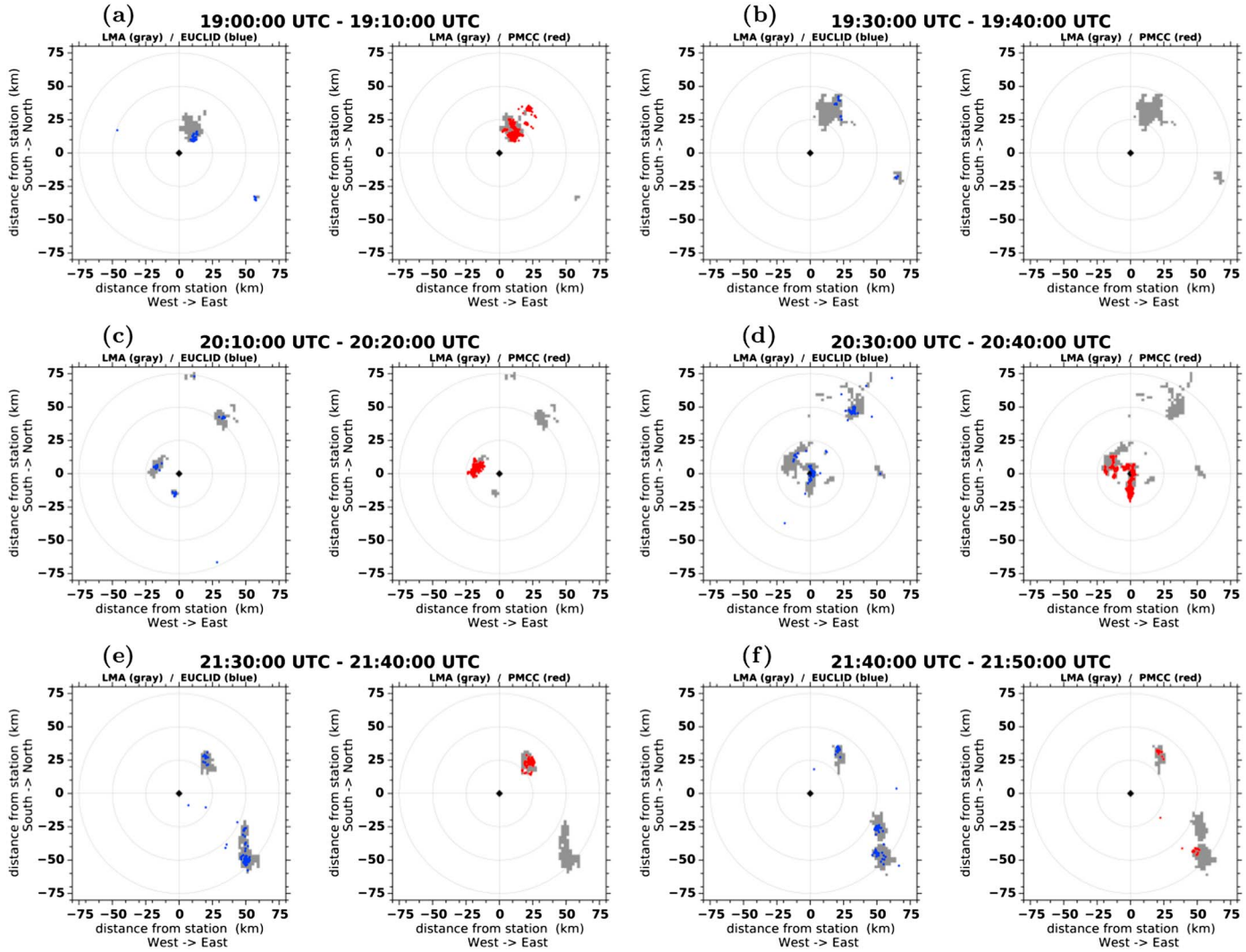

Figure 9. For six windows of 10 min duration during the thunderstorm from 18 UTC to 22 UTC, on the 26 October 2012: map of the HyLMA detections (gray regions) with the EUCLID observations (blue dots) and the reconstructed acoustic detections (red dots).

from the MPA, Figures 9e and 9f) was appearing in the southeast of the MPA at the end of the storm (around 21:30 UTC). Clearly it was acoustically detected (Figure 9f).

5. Statistics on the HyLMA and MPA Detections

5.1. Statistics on the Azimuths and the Horizontal Distances

The 56 selected flashes present enough data to establish statistical comparisons between HyLMA spatial points and reconstructed MPA detections. This comparison is illustrated in Figure 10.

At the end of the thunderstorm (from 21:30 UTC), a very active storm cell was building up at the southeast of the MPA (azimuth 135°) further than 50 km. The corresponding HyLMA detections are visible in Figure 10a through the highly populated bins between 105° and 150° and in Figure 10b between 50 km and 80 km. Due to the distance effect, few flashes in this active cell were detected by the MPA. Figures 10c and 10e prove that all the azimuths were swept by the flashes and all the azimuths were correctly detected by the MPA (as already pointed out before but on selected reconstruction cases). The shapes of the two distributions are very similar, with approximately equal proportions for the populations of the bins. This illustrates the fact that the efficiency of the acoustic method was uniform over the directions. One can conclude that when wind shears do not cancel the detectability, the wind direction does not modify strongly the acoustic reconstruction over the azimuths.

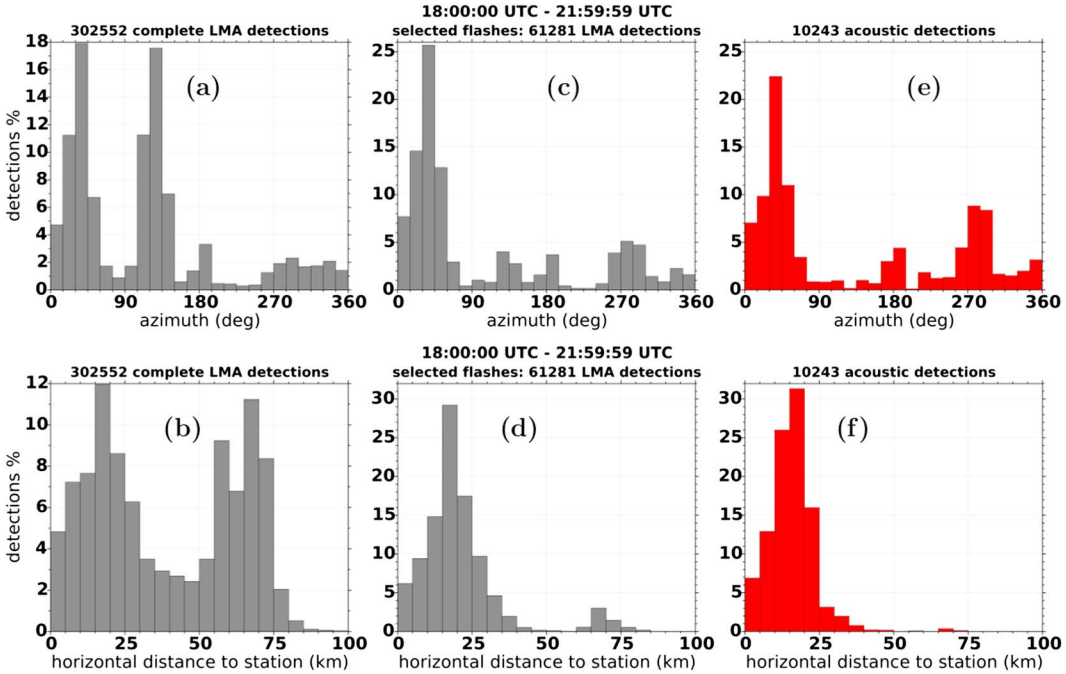

Figure 10. Global statistics from 18:00 UTC to 22:00 UTC, on 26 October 2012. Grey: HyLMA detections. Red: acoustic detections. (a, b) HyLMA detections for the complete ensemble of flashes detected by the HyLMA. (c, d) HyLMA detections associated with the 56 flashes which were detected by the acoustic method. (e, f) Reconstructed MPA detections associated to the 56 selected flashes. (a, c, and e) Distribution of azimuths around the MPA. (b, d, and f) distribution of horizontal distances from the MPA.

Figures 10d and 10f present histograms of the statistical distributions of the detections from the HyLMA and the MPA, when horizontal distances to the MPA are considered. For the flashes of less than 25 km distant from the MPA, the global shapes of the two distributions and the proportions of the populations in the bins are similar. Further than 25 km, the number of MPA detections falls below 3% (Figure 10f) and the bins proportions do not correspond anymore to those from the HyLMA distribution (Figure 10d). Nonetheless, for the flashes distant from 60 km to 80 km, there are some acoustic detections (less than 1%) which were correctly localized in horizontal distance.

5.2. Statistics on the Altitudes of the HyLMA and MPA Detections

Figure 11 shows the statistical distributions of the altitudes from the HyLMA detections, compared to the distribution of the reconstructed altitudes of the acoustic detections. Figures 11a and 11b compare the distributions from the complete set of HyLMA detections with the HyLMA detections from the selected flashes. These two distributions are clearly the same. The usual two layers of electrical activity [*Riousset et al.*, 2007] are

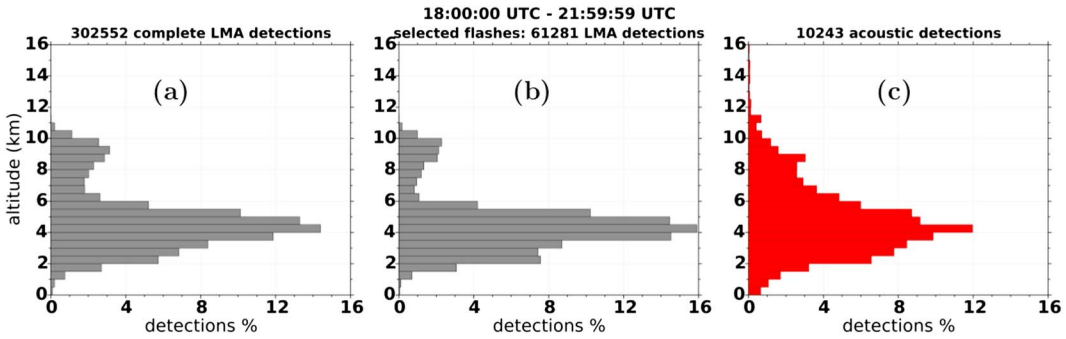

Figure 11. Global statistics from 18:00 UTC to 22:00 UTC, on 26 October 2012. Grey: HyLMA detections. Red: acoustic detections. Distributions of the altitudes of the detections, (a) HyLMA detections for the complete ensemble of flashes detected by the HyLMA. (b) HyLMA detections associated with the 56 flashes which were detected by the acoustic method. (c) Statistics for the reconstructed acoustic detections associated to the 56 selected flashes.

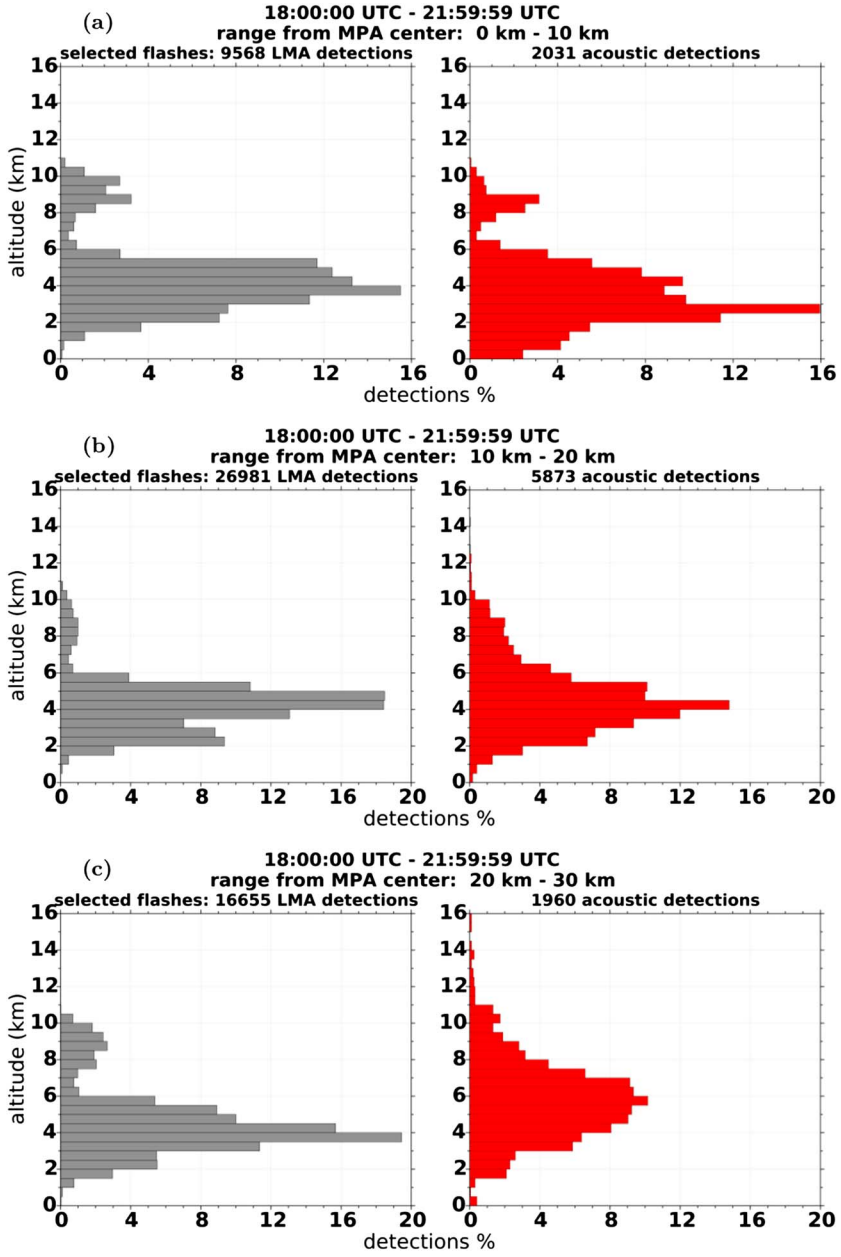

Figure 12. Global statistics from 18:00 UTC to 22:00 UTC, on 26 October 2012. Altitude of detections for different ranges of horizontal distance from MPA center. Grey: HyLMA detections for the 56 selected flashes. Red: corresponding reconstructed acoustic detections. (a) Range 0 km to 10 km. (b) Range 10 km to 20 km. (c) Range 20 km to 30 km.

visible, at about, respectively, 4 km and 9 km altitude. The distribution for reconstructed MPA detections is in Figure 11c. The shape of the distribution seems to be unimodal with a peak around 4 km, but a smaller peak could be present and partially masked at an altitude of 9 km. This distribution built from acoustic detections clearly differs from the ones from the HyLMA.

Figures 12a–12d are the distributions of altitudes from HyLMA and MPA detections, computed for different horizontal distance ranges from the MPA. In Figure 12a the distance range is from 0 km to up 10 km. In this case the acoustic method is able to detect two layers of discharges that are also described by the HyLMA. Indeed, the former is able to both resolve the layered intracloud activity and to clearly describe the lower part of the cloud-to-ground return strokes. The bins proportions between HyLMA and MPA detections are approximately the same, with neither having detections above 11 km.

When more distant sources are analyzed (Figures 12b and 12c), the acoustic method is not able anymore to differentiate the two layers of electrical activity. But these two layers are still present as showed by the HyLMA distribution. In this case of two layered lightning, the shape of the acoustic distribution is due to the acoustic detection method itself, which was affected by biases such as propagation effects.

The number of acoustic detections is 2031 for the ranges (0 km – 10 km) with a density of 6.4 detections per square kilometer. It is maximal for the ranges (10 km – 20 km) with a similar density (5873 detections, 6.2 detections per square kilometer). Then it falls off for greater distances (1960 detections for the ranges (20 km – 30 km), 1.2 detections per square kilometer).

Propagation effects can have strong impact on the detectability. One effect, which does not depend on azimuth, is that the typical decrease in temperature with height causes acoustic rays to curve upward [*Fleagle*, 1949], so rays from channel segments at low-elevation angles curve upward over the observer. A second effect depends on wind shear; it depends on azimuth relative to the wind and can have a much greater effect than the effect of the temperature gradient — it can be large enough to prevent one from hearing thunder from a flash only a few kilometers away. The attenuation by the atmosphere also affects the thunder that is heard. It tends to be greater for higher frequencies, thereby contributing to the decrease in amplitude and peak frequency of thunder signals. The authors' choice of an operating frequency range in the infrasonic to the lower part of the audible spectrum mitigates this effect of attenuation by the atmosphere itself. It can be concluded that the efficiency of the acoustic method is the highest for distances smaller than 20 km.

To our knowledge only *MacGorman et al.* [1981] presented such statistical study of reconstructed altitudes from acoustic detection of lightning. Figures 6 and 11 of their paper present a vertical distribution similar to the one presented in Figure 11c. *MacGorman et al.* [1981] also present Figures 7 and 13 where the distribution of altitudes appears to contain two peaks. At last, Figure 14 from their paper is based on data from another storm and also contains two peaks. The authors discussed that the challenge of explaining such differences between explored cases would be a difficult question. Electromagnetic localization tools like the HyLMA or EUCLID were not accessible at this time to *MacGorman et al.* [1981]. Therefore, they could not compare their results with data obtained from electromagnetic methods. Based on the compared electromagnetic-acoustic distributions from the present paper, one would be tempted to interpret that flashes reconstructed by *MacGorman et al.* [1981] from acoustic records presented a classic two-layer structure: the number of peaks in the distributions of altitudes being due to acoustic propagation (either using direct or ray tracing propagation, see the synthetic statistical distribution in Figure B4). Although being compatible with our observations, this explanation is debatable on several points. Data from *Teer and Few* [1974] show that the flashes studied by *MacGorman et al.* [1981] were comparably close to the microphone array, so the effect of propagation does not seem to explain simply the differences in vertical distribution of acoustic sources. *Bruning et al.* [2007] show a storm in which the vertical distribution of sources from an LMA has a single lower peak during part of its lifetime. At last histograms presented by *MacGorman et al.* [1981] are not sorted by horizontal distances, comparison of both studies is thus difficult. In our opinion it remains risky to compare and explain differences between our statistical studies and the ones from *MacGorman et al.* [1981].

The presented study will have to be performed on other cases selected in the 3 months observation period, to find out if the observed statistical distributions are general or were only specific to the studied case. This would allow one to explore storm to storm and time to time variations in the statistical distributions. More deeply, variations in the property lightning mapping systems detect (radar, acoustic, infrasound, VHF and VLF radiations, etc.) can affect the vertical distribution a system sees (e.g., the comparison of radar and acoustic detections by Holmes *et al.* in the late 1970s or early 1980s). So the fundamental challenge is in determining how the measured vertical distribution of lightning depends on the characteristics of the storm itself (the ultimate goal) and how it is affected by the system being used to measure it.

5.3. Acoustic Description of the Lower Parts of the CG Flashes

It is pointed out that a lot of acoustic detections are reconstructed below 2 km in altitude (Figure 12a). But this is not the case for the HyLMA detections as already noted in section 4.1: there are very few HyLMA detections below 1 km altitude (Figures 11a, 11b, and 12a – 12d). In this section the attention is focused on the ability of the acoustic method to describe lower parts of CGs near the MPA, below 2 km height. For these altitudes, the performance of the HyLMA strongly decreases.

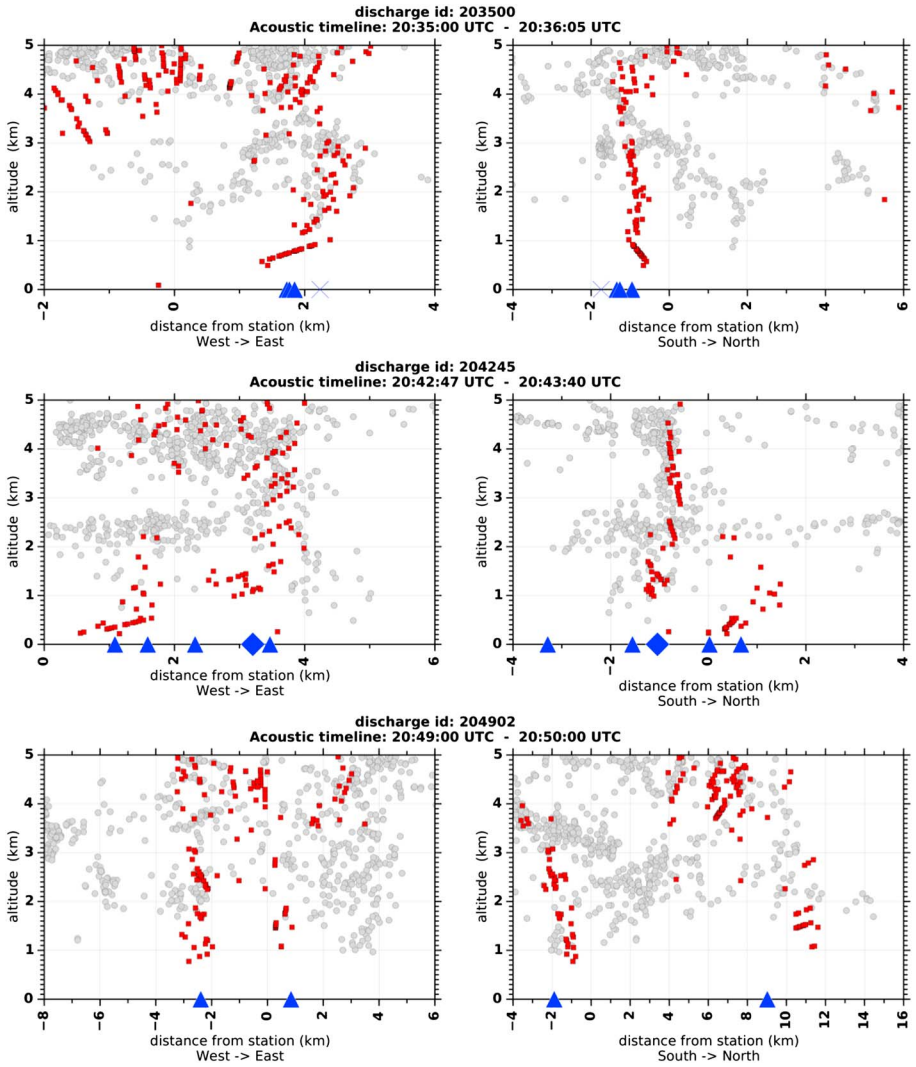

Figure 13. Comparison of the detection capabilities of the HyLMA (gray points) and the reconstructed acoustic sources (red squares) for lower altitudes (under 5 km height). The blue symbols are the EUCLID observations (same symbols as in Figure 4). Each line: cases of the CGs which occurred at 20:35:00 UTC, 20:42:45 UTC, and 20:49:02 UTC. The MPA is at the origin. (left column) Projections in the west to east direction. (right column) Projections in the south to north direction.

An LMA needs line of sight to the source of the VHF radiation in order to be able to locate it. Because of the mountainous terrain of the HyMeX area, the lower parts of the CG channels were not seen by the required minimum of six HyLMA stations to be located. This is why the HyLMA did not locate the near-ground channels, while the MPA was able to locate them. Figure 13 illustrates this with the case of three flashes where CGs were present within 10 km from the station. The characteristics of the associated EUCLID observations are in Table 5.

The case of the flash of 20:35:00 UTC has already been presented. Here the zoom on the lower altitudes clearly shows that the acoustic method was able to correctly detect the parts of the return strokes below 1 km. There are few HyLMA detections for these altitudes, they are much more diffuse and they are not clearly associated to the EUCLID observations (contrary to the acoustic detections).

For the flash which occurred at 20:42:45, the south to north projection shows that the acoustic detections followed the part of the discharge from 5 km altitude to 1 km (it appears vertical in this projection). The acoustic method did not describe the lower horizontal layer around 2 km altitude, but no thunder was detected from much of the horizontal structure around 2 km altitude, possibly because the amplitude of thunder from that horizontal structure was less than the amplitude from more vertical channels. On the west to east view, the lightning channel was tilted. The acoustic detections are distributed over the EUCLID ones.

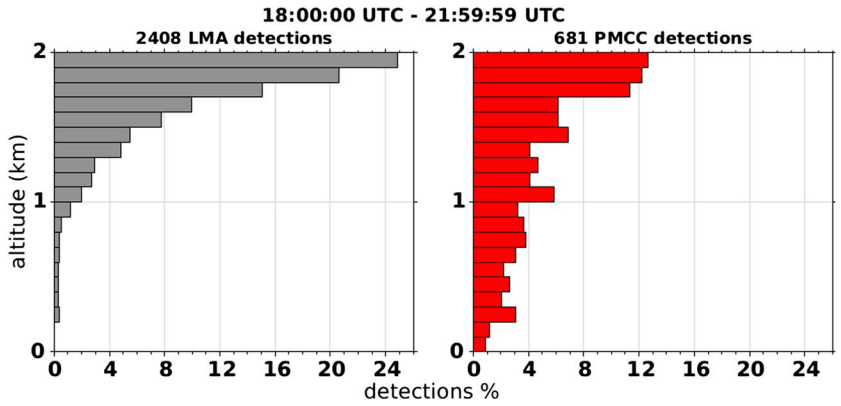

Figure 14. Among the 56 flashes which were detected both by the HyLMA and the acoustic network, 50 of them present at least one EUCLID observation with connection to the ground. (left) Distribution between 0 km and 2 km in altitude of the HyLMA detections associated for these 50 CGs. (right) Altitudes of the reconstructed acoustic detections for these same 50 CGs.

At last, the example of the flash of 20:49:02 shows that the acoustic detections are separated into two groups, each one being associated to an EUCLID negative CG. There is no MPA nor HyLMA detection below 500 m altitude. The parts of the return strokes below 500 m are about 2 km and 10 km from the MPA; thus, (following *Fleagle* [1949] results) the associated acoustic sources are likely to be in the shadow zone.

Figure 14 presents a global statistic for the altitudes below 2 km, for the 50 reconstructed lightning flashes which presented at least one connection to the ground. The ratio of detections is about 3.5 (2408 HyLMA detections against 681 MPA detections). It is clear that the detection capabilities of the HyLMA decreases exponentially as the altitude decreases. There are less than 2% of HyLMA detections below 1 km height. On the contrary, the number of acoustic detections decreases approximately linearly as the altitude goes down. The complementarity of an acoustic detection system along with an electromagnetic one, especially to reconstruct lower parts of nearby CGs below 2 km height, is thus demonstrated.

6. Conclusions

This article investigates the acoustical detection and reconstruction of natural lighting, using a 2 months long recording period by an acoustic station of four microphones (MPA) located in south of France during fall 2012. This observation program took place within the European project HyMeX. Given the large number of recordings, the study permits a statistical analysis beyond the reconstruction of individual flashes. The acoustical analysis is compared to very high frequency electromagnetic detection by a Lighting Mapping Array (HyLMA) of 12 antennas installed during the same period of time. These data are supplemented by those from the low-frequency lightning location system EUCLID. Our study focused on a storm that passed over the acoustic station at 18:00–22:00 UTC on 26 October 2012. This storm was chosen because it produced a sufficient number of flashes distributed at all azimuths from the acoustic station but had a small enough flash rate that the thunder produced by sequential flashes did not usually overlap. The postprocessing of acoustical data in the frequency range 1 to 40 Hz using PMCC turned out successfully, even though PMCC is most routinely used for lower frequency, infrasonic signals. Using (1) the azimuth and elevation from which an acoustic signal arrived at the MPA, (2) the time of propagation given by the difference between the time a flash was detected by the HyLMA and the time the acoustic signal arrived at the MPA, (3) a simple assumption of acoustic propagation in straight line with uniform speed of sound of 340 m/s; tridimensional geometrical reconstructions of 56 lightning discharges were carried out.

The correlation between acoustic and electromagnetic HyLMA reconstructions turns out very satisfactory in azimuth, elevation angle, and horizontal distance for discharges less than 25 km away from the acoustic station. For larger distances, the acoustic array can detect some of the remote flashes, up to 75 km in this study. The correlations between acoustic and electromagnetic data show that the number of acoustic detections and the resolution of the acoustic reconstructions deteriorate as the distance from the MPA increases, still with good correlation in azimuth and horizontal distances.

For lightning strokes at less than 10 km away from the MPA, there is a good agreement for the altitude between reconstructed acoustic sources and HyLMA ones. At such small distances, the acoustic method has been shown to be able to differentiate the two levels of discharges inside the clouds, in addition to cloud-to-ground strokes (CGs). It seems that MPA was more sensitive to vertical IC discharges. Note, however, that if acoustic signals from two sources arrive at the MPA at the same time, only the source of the most intense signal can be reconstructed (if a source can be determined at all), and this can create gaps in the reconstructed lightning structure. For more remote lightning flashes, altitudes of the reconstructed acoustic sources are overestimated as the distance increases.

Moreover, the ability of the acoustic method to describe in detail the lower part of nearby CGs, below 2 km altitude is demonstrated, while HyLMA is not efficient under these conditions. The ground connection of the acoustically reconstructed channels matches very well with the localization of EUCLID observations.

For nearby flashes, the use of meteorological profiles therefore does not appear necessary to correctly reconstruct the geometries of the discharges. For more distant flashes, influence of meteorological situation (wind and temperature gradient) on the performances of the altitude localization process remains to be further investigated in a statistical way. Characterization of lightning as acoustical sources in terms of frequency, pressure amplitude, and energy will also be further explored using the present HyMeX data.

Appendix A: Naming and Plotting Conventions

A1. List of Acronyms Used in the Paper

AROME: operational weather forecast model from Météo-France [*Seity et al.*, 2011].
AROME-WMED: AROME West-MEDiterranean region [*Fourrié et al.*, 2015], version of AROME specifically adapted for HyMeX.
CG: cloud-to-ground discharge.
EUCLID: European Cooperation for Lightning Detection [*Schulz et al.*, 2014a, 2014b]. Operational lightning location network providing detection data in the very low to low electromagnetic frequency range up to 350 kHz.
HyMeX: Hydrological Cycle in the Mediterranean Experiment [*Drobinski et al.*, 2014]. European project aiming at enhancing the understanding and description of the water cycle and its variabilities in the Mediterranean region.
HyLMA: HyMeX Lightning Mapping Array installed for the SOP1 campaign. See section 2.1 and Figure 1.
IC: intracloud discharge.
LMA: Lightning Mapping Array, very high frequency (60 MHz–66 MHz) lightning detection network.
MBA: microbarometer array. Four microbarometers organized as a triangle of 500 m side. See section 2.1 and Figure 1.
MPA: microphone array. Four microphones organized as a triangle of 50 m side centered around the MPA. See section 2.1 and Figure 1.
SOP1: Special Observation Period 1. Observation campaign that took place within HyMeX in autumn 2012 (from September 5 2012 to November 6 2012) in the southeast of France.

A2. List of Symbols Used in the Figures

Acoustic detections: represented with red square symbols.
EUCLID detections: presented with the following blue symbols, triangle symbol: negative CG, cross: positive CG, diamond: negative IC, star: positive IC.
HyLMA detections: plotted using circles filled with grey.

Appendix B: Reconstruction of Lightning Flashes With a Ray Tracing Method

We use in this paper a direct reconstruction method. Each acoustic source, detected by PMCC, has its time of occurrence, t_{PMCC}, azimuth θ_S, and elevation angle ϕ_S (via the trace velocity measurement). We calculate the time of propagation Δt as the difference of t_{PMCC} and the time of the first discharge of a flash measured by HyLMA. In this appendix, we reconstruct the localization of the acoustic sources using a ray tracing method.

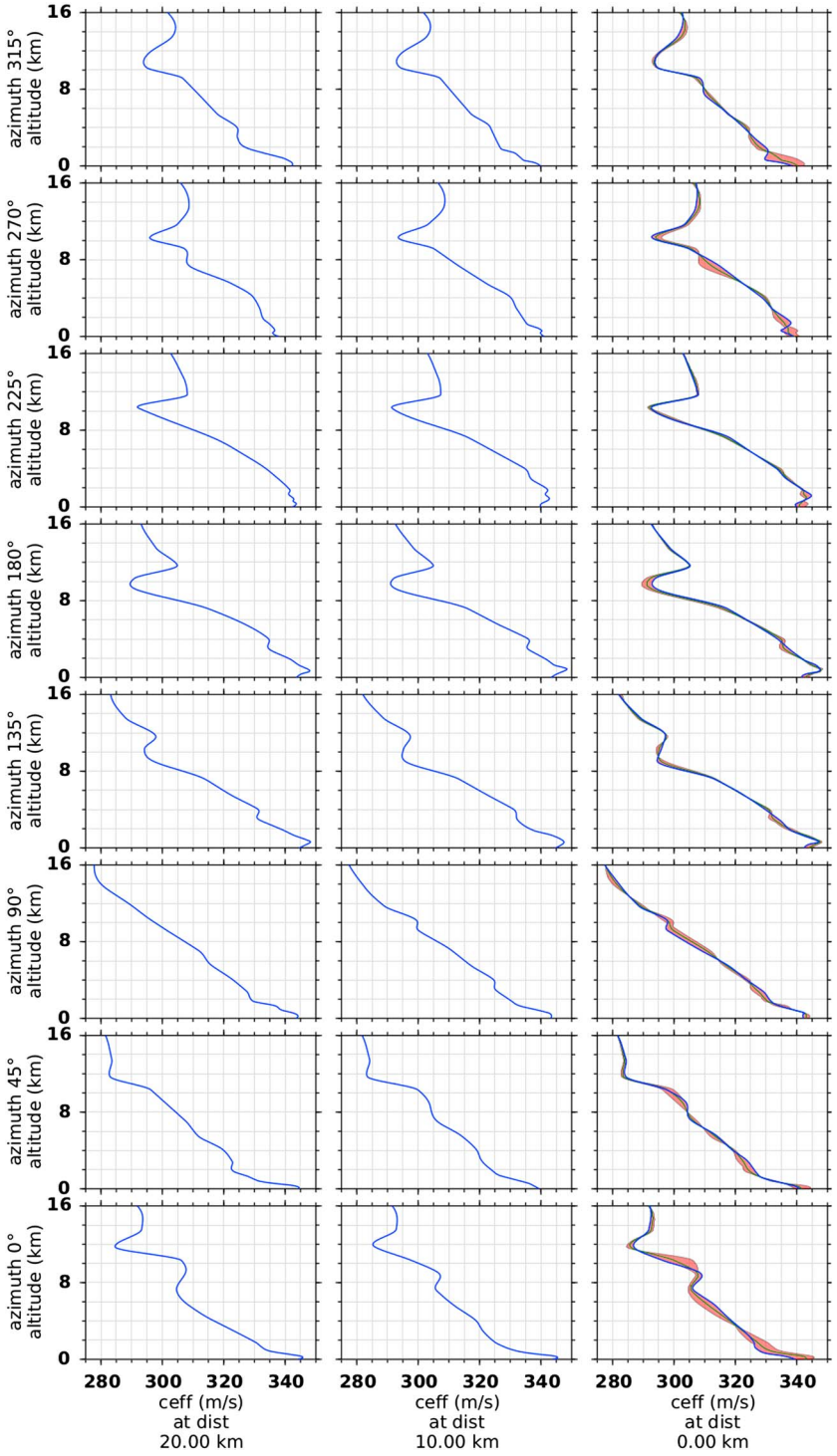

Figure B1. Outputs of the AROME-WMED software for 26 October 2012 at 20:00 UTC. Profiles of the effective sound speed seen by a wavefront propagating *from a source* at different azimuths and distances from the MPA *toward* the MPA. The profiles over the station are presented on the right column.

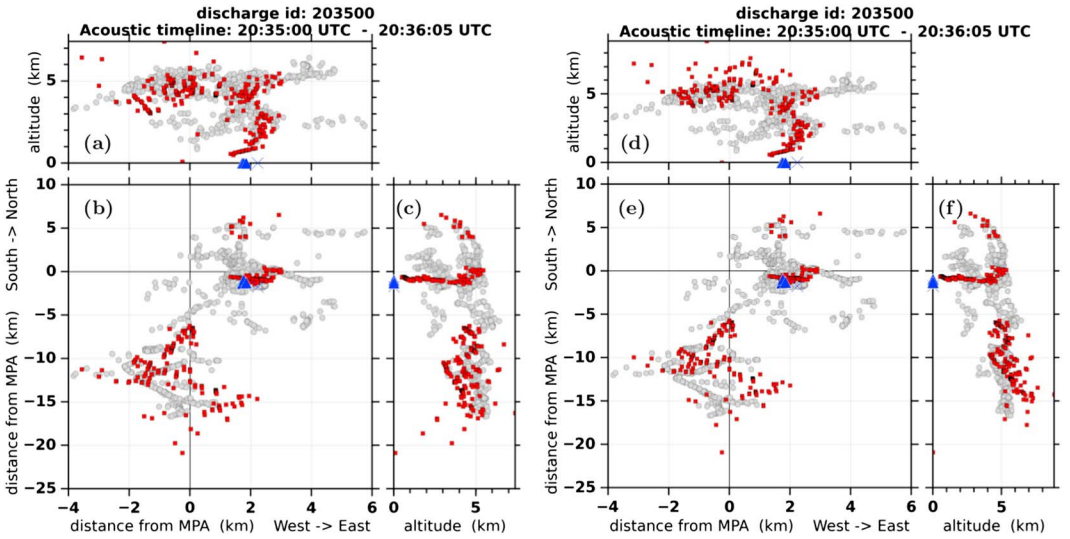

Figure B2. Acoustic reconstruction of the flash occurred the 26 October 2012 at 20:35:00 UTC. Comparison between (a–c) reconstruction with direct propagation and (d–f) reconstruction with ray tracing through AROME-WMED meteo profile (with temperature and wind). (a, d) Locations of HyLMA detections, EUCLID observations, and reconstructed MPA detections in longitude-altitude plane. (b, e) In longitude-latitude plane (MPA is at the origin). (c, f) In altitude-latitude plane.

The inputs of this calculation are the parameters of each acoustic source Δt, θ_s, and ϕ_s (the same used in the direct propagation method) and the meteorological profiles which are the outputs of the AROME-WMED software (Figure B1).

But in severe weather environments with strong updrafts, downdrafts, and outflow boundaries, vertical wind and temperature profiles cannot be typically obtained with enough spatial or temporal resolution to initialize ray tracing computations. In addition, recent measurements of the wind during a thunderstorm, using Doppler sounder [*Thobois and Soderholm*, 2015], showed spatial and temporal structures which are absolutely not resolved by the AROME-WMED software. Figures B2 and B3 show the acoustic reconstruction for two flashes which occurred on 26 October 2012 at 20:35:00 UTC and 21:16:54 UTC using ray tracing method and direct propagation method. One can see that when the flash is close to MPA (about 2 km for the return strokes

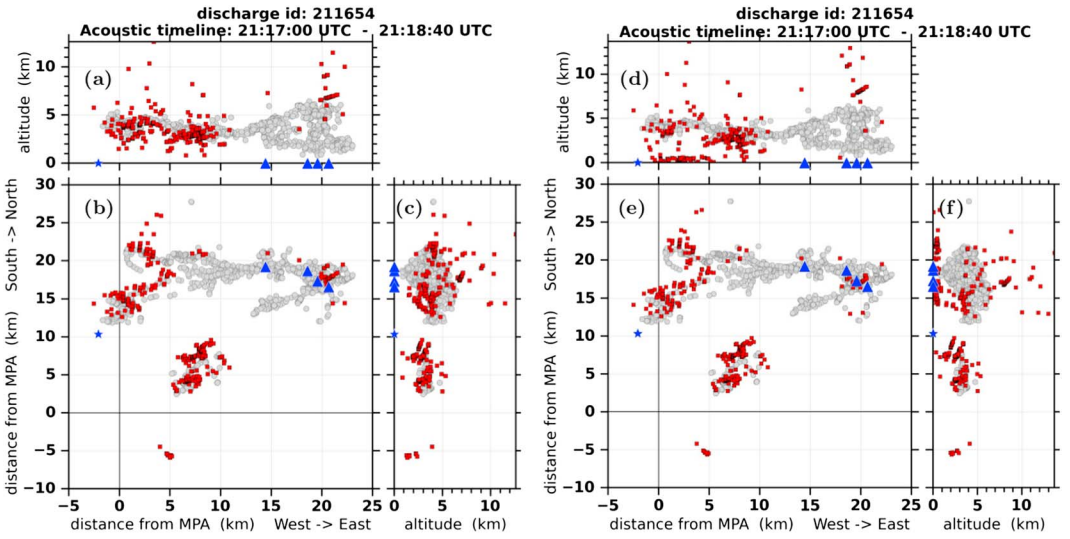

Figure B3. Acoustic reconstruction of the flashes occurred on 26 October 2012 at 21:16:54 UTC. Comparison between (a–c) reconstruction with direct propagation and (d–f) reconstruction with ray tracing through AROME-WMED meteo profile (with temperature and wind). Same legend as in Figure B2.

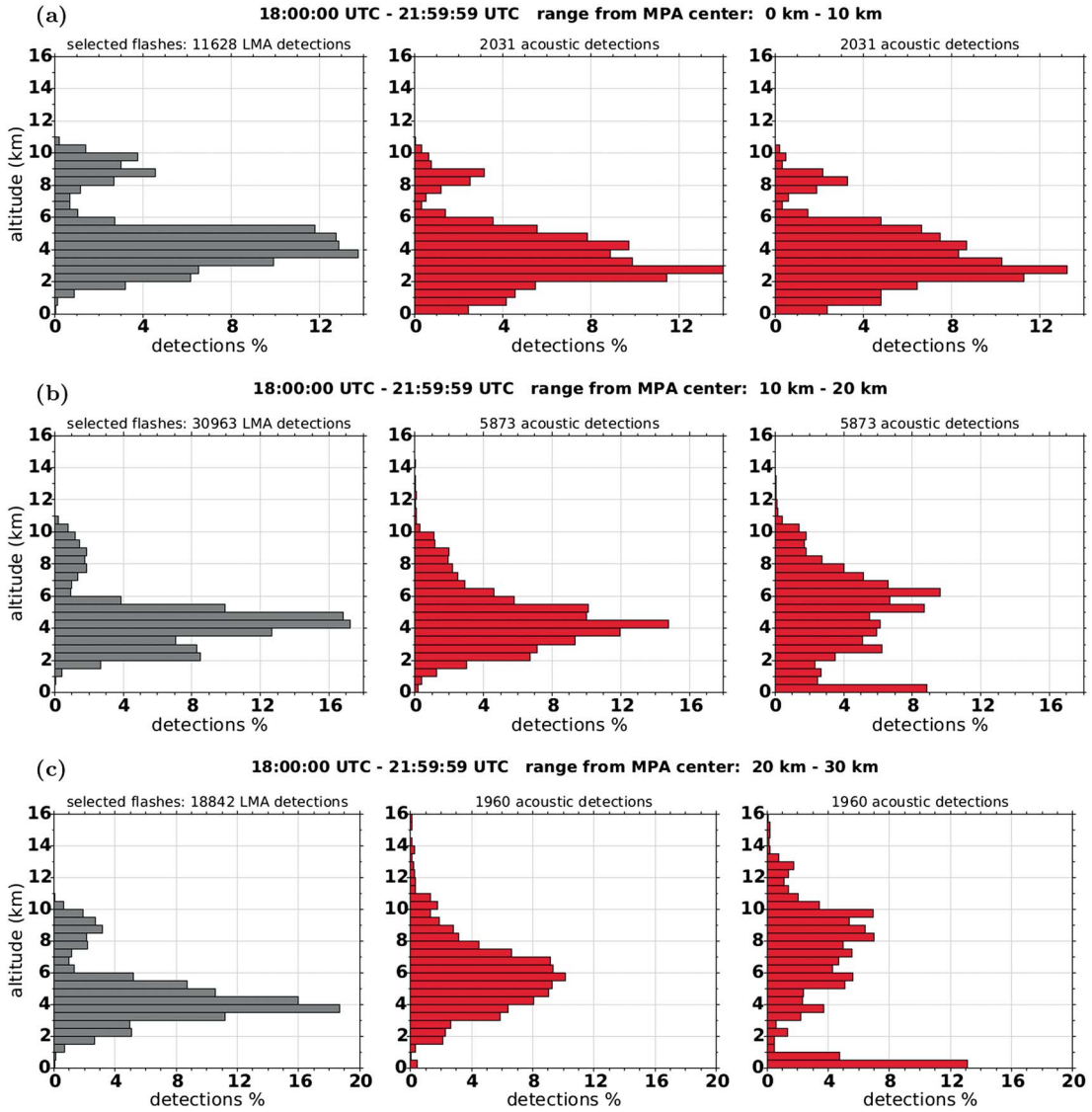

Figure B4. Global statistics from 18:00 UTC to 22:00 UTC, on 26 October 2012. (left column) HyLMA detections. (middle column) Acoustic detections reconstructed with direct propagation (corresponding to Figure 12). (right column) Acoustic detections reconstructed using ray tracing with wind and temperature gradients. (a) Range 0 km to 10 km. (b) Range 10 km to 20 km. (c) Range 20 km to 30 km.

at 20:35:00 UTC, see Table 5), results from the two reconstruction methods are quite close. But, when the flash is farther (about 26 km for the return strokes at 21:16:54 UTC, see Table 5), one can see that numerous acoustic sources coming northward are located at ground level with the ray tracing method, while they are reasonably localized in the thundercloud by the direct propagation method. The presence of a small wave guide observed in that direction below 2 km height (Figure B1, lower right plot) could be the reason of this bad result from the ray tracing method. Figure B4 (third column) shows the distributions of altitudes from the 56 MPA detections, computed for different horizontal distance ranges from the MPA using the ray tracing method. By comparison with the Figure 12 (that corresponds to Figure B4 (second column)) which was obtained using the direct propagation method, one can see that for distances lower than 10 km, both distributions are quite close. This comparison for distributions of altitudes of acoustic discharges for lightning flashes located from 10 km to 20 km (Figure B4b) or from 20 km to 30 km (Figure B4c) let appear a large proportion of acoustic sources at ground level for the ray tracing method which are absolutely not present in Figures 12b and 12c. For distances from 20 km to 30 km, the distribution peak for the statistics from ray tracing is shifted toward higher altitudes and is broadened when compared to the distribution from straight-line reconstruction.

Acknowledgments
The authors are grateful to the CEA technical team who deployed and maintained the acoustic station during the SOP1. Alexis Le Pichon (CEA) is thanked for his help on the postprocessing of the acoustic records from the MPA and the MBA. The SOP1 was funded by grants MISTRALS/HYMEX and ANR-11-BS56-0005 IODA-MED. The authors acknowledge Meteo-France and the HyMeX program for supplying the data, sponsored by grants MISTRALS/HyMeX and ANR-11-BS56-0005 IODA-MED project. Present results have been obtained within the frame of the LETMA (Laboratoire ETudes et Modélisation Acoustique), Contractual Research Laboratory between CEA, CNRS, Ecole Centrale Lyon, C-Innov, and Université Pierre et Marie Curie. The acoustic signals and the HyLMA and EUCLID data are available on the HyMeX database (http://mistrals.sedoo.fr/HyMeX/). The PMCC software is developed by the CEA. The authors are also grateful to the anonymous reviewers for their helpful comments and valuable suggestions.

References

Alcoverro, B., and A. Le Pichon (2005), Design and optimization of a noise reduction system for infrasonic measurements using elements with low acoustic impedance, *J. Acoust. Soc. Am.*, *117*(4), 1717–1727.

Anderson, J. F., J. B. Johnson, R. O. Arechiga, and R. J. Thomas (2014), Mapping thunder sources by inverting acoustic and electromagnetic observations, *J. Geophys. Res. Atmos.*, *119*, 13,287–13,304, doi:10.1002/2014JD021624.

Arechiga, R., J. B. Johnson, H. E. Edens, R. J. Thomas, and W. Rison (2011), Acoustic localization of triggered lightning, *J. Geophys. Res.*, *116*, D09103, doi:10.1029/2010JD015248.

Arechiga, R., M. Stock, R. Thomas, H. Erives, W. Rison, H. Edens, and J. Lapierre (2014), Location and analysis of acoustic infrasound pulses in lightning, *Geophys. Res. Lett.*, *41*, 4735–4744, doi:10.1002/2014GL060375.

Assink, J. D., L. G. Evers, I. Holleman, and H. Paulssen (2008), Characterization of infrasound from lightning, *Geophys. Res. Lett.*, *35*, L15802, doi:10.1029/2008GL034193.

Bodhika, J. A. P., W. G. D. Dharmarathna, M. Fernando, and V. Cooray (2013), Reconstruction of lightning channel geometry by localizing thunder sources, *J. Atmos. Sol. Terr. Phys.*, *102*, 81–90.

Brachet, N., D. Brown, R. Le Bras, Y. Cansi, P. Mialle, and J. Coyne (2009), Monitoring the Earth's atmosphere with the global IMS infrasound network, in *Infrasound Monitoring for Atmospheric Studies*, edited by A. Le Pichon, E. Blanc, and A. Hauchecorne, pp. 77–118, Springer, Dordrecht, Netherlands.

Bruning, E. C., W. D. Rust, T. J. Schuur, D. R. MacGorman, P. R. Krehbiel, and W. Rison (2007), Electrical and polarimetric radar observations of a multicell storm in TELEX, *Mon. Weather Rev.*, *135*(7), 2525–2544.

Caljé, L. (2005), Exploring boundaries of the Fisher and PMCC signal-detectors using infrasound signals, Master's thesis, Utrecht Univ., Utrecht, Netherlands.

Cansi, Y. (1995), An automatic seismic event processing for detection and location: The P.M.C.C. method, *Geophys. Res. Lett.*, *22*(9), 1021–1024.

Cansi, Y., and A. Le Pichon (2009), Infrasound event detection using the progressive multi-channel correlation algorithm, in *Handbook of Signal Processing in Acoustics*, edited by Y. Cansi and A. Le Pichon, pp. 1425–1435, Springer, New York.

Defer, E., et al. (2015), An overview of the lightning and atmospheric electricity observations collected in southern France during the HYdrological cycle in Mediterranean EXperiment (HyMeX), Special Observation Period 1, *Atmos. Meas. Tech.*, *8*(2), 649–669.

Dietrich, S., D. Casella, F. Di Paola, M. Formenton, A. Mugnai, and P. Sanò (2011), Lightning-based propagation of convective rain fields, *Nat. Hazards Earth Syst. Sci.*, *11*(5), 1571–1581.

Drobinski, P., et al. (2014), HyMeX: A 10-year multidisciplinary program on the mediterranean water cycle, *Bull. Am. Meteorol. Soc.*, *95*(7), 1063–1082.

Ducrocq, V., et al. (2014), HyMeX-SOP1: The field campaign dedicated to heavy precipitation and flash flooding in the northwestern Mediterranean, *Bull. Am. Meteorol. Soc.*, *95*(7), 1083–1100.

Farges, T., and E. Blanc (2010), Characteristics of infrasound from lightning and sprites near thunderstorm areas, *J. Geophys. Res.*, *115*, A00E31, doi:10.1029/2009JA014700.

Few, A. A. (1968), Thunder, PhD thesis, Rice Univ., Houston, Tex.

Few, A. A. (1969), Power spectrum of thunder, *J. Geophys. Res.*, *74*(28), 6926–6934.

Few, A. A. (1970), Lightning channel reconstruction from thunder measurements, *J. Geophys. Res.*, *75*(36), 7517–7523.

Few, A. A. (1986), Acoustic radiations from lightning, in *The Earth Electrical Environment*, edited by E. P. Krider, chap. 4, pp. 40–60, Natl. Acad. Press, Washington, D. C.

Few, A. A., and T. L. Teer (1974), The accuracy of acoustic reconstructions of lightning channels, *J. Geophys. Res.*, *79*, 5007–5011.

Fleagle, R. G. (1949), The audibility of thunder, *J. Acoust. Soc. Am.*, *21*(4), 411–412.

Fourrié, N., et al. (2015), AROME-WMED: A real-time mesoscale model designed for the HyMeX special observation periods, *Geosci. Model Dev. Discuss.*, *8*, 1801–1856.

Gallin, L.-J., M. Rénier, E. Gaudard, R. Marchiano, F. Coulouvrat, and T. Farges (2014), One-way approximation for the simulation of weak shock wave propagation in atmospheric flows, *J. Acoust. Soc. Am.*, *135*(5), 2559–2570.

Hedlin, M. A. H., B. Alcoverro, and G. D'Spain (2003), Evaluation of rosette infrasonic noise-reducing spatial filters, *J. Acoust. Soc. Am.*, *114*(4), 1807–1820.

Holmes, C. R., M. Brook, P. Krehbiel, and R. McCrory (1971), On the power spectrum and mechanism of thunder, *J. Geophys. Res.*, *76*(9), 2106–2115.

Johnson, J. B., R. O. Arechiga, R. J. Thomas, H. E. Edens, J. Anderson, and R. Johnson (2011), Imaging thunder, *Geophys. Res. Lett.*, *38*, L19807, doi:10.1029/2011GL049162.

Koshak, W. J., et al. (2004), North Alabama Lightning Mapping Array (LMA): VHF source retrieval algorithm and error analyses, *J. Atmos. Oceanic Technol.*, *21*(4), 543–558.

Krehbiel, P. R., R. J. Thomas, W. Rison, T. Hamlin, J. Harlin, and M. Davis (2000), GPS-based mapping system reveals lightning inside storms, *Eos Trans. AGU*, *81*, 21–25.

Le Pichon, A., R. Matoza, N. Brachet, and Y. Cansi (2010), Recent enhancements of the PMCC infrasound signal detector, *Inframatics Newsl.*, *26*, 1–8.

MacGorman, D. R., A. A. Few, and T. L. Teer (1981), Layered lightning activity, *J. Geophys. Res.*, *86*(C10), 9900–9910.

Pasko, V. P. (2009), Mechanism of lightning-associated infrasonic pulses from thunderclouds, *J. Geophys. Res.*, *114*, D08205, doi:10.1029/2008JD011145.

Pineda, N., T. Rigo, J. Bech, and X. Soler (2007), Lightning and precipitation relationship in summer thunderstorms: Case studies in the North Western Mediterranean region, *Atmos. Res.*, *85*(2), 159–170.

Ponceau, D., and L. Bosca (2009), Low-noise broadband microbarometers, in *Infrasound Monitoring for Atmospheric Studies*, edited by A. Le Pichon, E. Blanc, and A. Hauchecorne, pp. 119–140, Springer, Dordrecht, Netherlands.

Qiu, S., B.-H. Zhou, and L.-H. Shi (2012), Synchronized observations of cloud-to-ground lightning using VHF broadband interferometer and acoustic arrays, *J. Geophys. Res.*, *117*, D19204, doi:10.1029/2012JD018542.

Rakov, V. A., and M. A. Uman (2003), Lightning: Physics and Effects.

Riousset, J. A., V. P. Pasko, P. R. Krehbiel, R. J. Thomas, and W. Rison (2007), Three-dimensional fractal modeling of intracloud lightning discharge in a New Mexico thunderstorm and comparison with lightning mapping observations, *J. Geophys. Res.*, *112*, D15203, doi:10.1029/2006JD007621.

Rison, W., R. J. Thomas, P. R. Krehbiel, T. Hamlin, and J. Harlin (1999), A GPS-based three-dimensional lightning mapping system: Initial observations in central New Mexico, *Geophys. Res. Lett.*, *26*(23), 3573–3576.

Schulz, W., D. Poelman, S. Pedeboy, C. Vergeiner, H. Pichler, G. Diendorfer, and S. Pack (2014a), Performance validation of the European lightning location system EUCLID, paper presented at International Colloquium on Lightning and Power Systems, Lyon, France, 12–14 May.

Schulz, W., S. Pedeboy, C. Vergeiner, E. Defer, and W. Rison (2014b), Validation of the EUCLID LLS during HyMeX SOP1, paper presented at 23rd International Lightning Detection Conference and 5th International Lightning Meteorology Conference, Tucson, Ariz., 18–21 Mar.

Seity, Y., P. Brousseau, S. Malardel, G. Hello, P. Bénard, F. Bouttier, C. Lac, and V. Masson (2011), The AROME-France convective scale operational model, *Mon. Weather Rev.*, *139*, 976–999.

Teer, T. L., and A. A. Few (1974), Horizontal lightning, *J. Geophys. Res.*, *79*(24), 3436–3441.

Thobois, L., and J. Soderholm (2015), *Nowcasting Severe Storms - Observing Clear Air Close Proximity Environment of Severe Storms*, Meteorol. Technol. Int., pp. 132–135, UKIP Media & Events Ltd., Dorking, U. K.

Thomas, R. J., P. R. Krehbiel, W. Rison, S. J. Hunyady, W. P. Winn, T. Hamlin, and J. Harlin (2004), Accuracy of the Lightning Mapping Array, *J. Geophys. Res.*, *109*, D14207, doi:10.1029/2004JD004549.

Walker, K. T., and M. A. H. Hedlin (2009), A review of wind-noise reduction methodologies, in *Infrasound Monitoring for Atmospheric Studies*, edited by A. Le Pichon, E. Blanc, and A. Hauchecorne, pp. 141–182, Springer, Dordrecht, Netherlands.